

A Keck HIRES Doppler Search for Planets Orbiting Metal-Poor Dwarfs. II. On the Frequency of Giant Planets in the Metal-Poor Regime

Alessandro Sozzetti^{1,2}, Guillermo Torres¹, David W. Latham¹, Robert P. Stefanik¹, Sylvain G. Korzennik¹, Alan P. Boss³, Bruce W. Carney⁴, and John B. Laird⁵

asozzett@cfa.harvard.edu

gtorres@cfa.harvard.edu

dlatham@cfa.harvard.edu

skorzennik@cfa.harvard.edu

rstefanik@cfa.harvard.edu

boss@dtm.ciw.edu

bruce@physics.unc.edu

laird@bgsu.edu

ABSTRACT

We present an analysis of three years of precision radial velocity measurements of 160 metal-poor stars observed with HIRES on the Keck 1 telescope. We report on variability and long-term velocity trends for each star in our sample. We identify several long-term, low-amplitude radial-velocity variables worthy of follow-up with direct imaging techniques. We place lower limits on the detectable companion mass as a function of orbital period. Our survey would have detected, with

¹Harvard-Smithsonian Center for Astrophysics, 60 Garden Street, Cambridge, MA 02138 USA

²INAF - Osservatorio Astronomico di Torino, 10025 Pino Torinese, Italy

³Department of Terrestrial Magnetism, Carnegie Institution of Washington, 5241 Broad Branch Road, NW, Washington, DC 20015 USA

⁴Department of Physics & Astronomy, University of North Carolina at Chapel Hill, Chapel Hill, NC 27599 USA

⁵Department of Physics & Astronomy, Bowling Green State University, Bowling Green, OH 43403 USA

a 99.5% confidence level, over 95% of all companions on low-eccentricity orbits with velocity semi-amplitude $K \gtrsim 100 \text{ m s}^{-1}$, or $M_p \sin i \gtrsim 3.0 M_J (P/\text{yr})^{(1/3)}$, for orbital periods $P \lesssim 3 \text{ yr}$. None of the stars in our sample exhibits radial-velocity variations compatible with the presence of Jovian planets with periods shorter than the survey duration. The resulting average frequency of gas giants orbiting metal-poor dwarfs with $-2.0 \lesssim [\text{Fe}/\text{H}] \lesssim -0.6$ is $f_p < 0.67\%$ (at the 1σ confidence level). We examine the implications of this null result in the context of the observed correlation between the rate of occurrence of giant planets and the metallicity of their main-sequence solar-type stellar hosts. By combining our dataset with the Fischer & Valenti (2005) uniform sample, we confirm that the likelihood of a star to harbor a planet more massive than Jupiter within 2 AU is a steeply rising function of the host’s metallicity. However, the data for stars with $-1.0 \lesssim [\text{Fe}/\text{H}] \lesssim 0.0$ are compatible, in a statistical sense, with a constant occurrence rate $f_p \simeq 1\%$. Our results can usefully inform theoretical studies of the process of giant planet formation across two orders of magnitude in metallicity.

Subject headings: planetary systems: formation — stars: statistics — stars: abundances — techniques: radial velocities

1. Introduction

Fourteen years after the Doppler detection of the Jupiter-mass planet around the nearby, solar-type star 51 Peg (Mayor & Queloz 1995), extrasolar planet discoveries have been reported by teams using four different techniques. Decade-long, high-precision ($3\text{-}5 \text{ m s}^{-1}$) radial-velocity surveys of ~ 2500 F-G-K dwarfs and sub-giants in the solar neighborhood¹ ($d \lesssim 30 - 50 \text{ pc}$) have yielded so far the overwhelming majority of the objects in the present sample (340 planets in ~ 270 systems, as of February 2009). Ground-based photometric transit surveys (for a review see for example Charbonneau et al. 2007, and references therein) are now uncovering new transiting systems at a rate of ~ 20 per year, and there are very bright prospects for an even steeper increase in the detection rate thanks to large surveys with space-borne observatories, which are currently ongoing (*CoRoT*; Baglin et al. 2002) or will start in the near future (*Kepler*; Borucki et al. 2003). Finally, an additional dozen or so sub-stellar companions have also been detected recently by means of gravitational microlensing (e.g., Bond et al. 2004; Beaulieu et al. 2006; Gaudi et al. 2008) as well

¹For reviews of the status of the most successful Doppler surveys for planets see for example Butler et al. (2006) and Udry & Santos (2007) and references therein, or Jean Schneider’s website <http://exoplanet.eu>.

direct imaging (e.g., Chauvin et al. 2005; Neuhäuser et al. 2005; Kalas et al. 2008; Marois et al. 2008) surveys, or timing of stellar oscillations (Silvotti et al. 2007; Lee et al. 2009).

The aims of Doppler surveys for planets have evolved in the recent past. On the one hand, existing surveys are extending their time baseline and/or are achieving higher velocity precision ($\lesssim 1 \text{ m s}^{-1}$, see for example Lovis et al. 2006), to continue searching for planets at increasingly larger orbital distances (e.g., Fischer et al. 2007) and with increasingly smaller masses (e.g., Udry et al. 2007; Mayor et al. 2008). On the other hand, early evidence for a strong relationship between the physical properties of stars and the likelihood that they harbor planets has prompted both theoretical analyses attempting to reconcile the observed trends within the framework of planet formation models as well as renewed experimental efforts to put such trends on firmer statistical grounds and thus thoroughly test the theoretical explanations put forth to explain their existence.

For example, if the surface density of solids in a protoplanetary disk is proportional to the mass of the central star, then, within the framework of the core accretion model of giant planet formation (e.g., Pollack et al. 1996; Alibert et al. 2005), one would expect a positive correlation between the mass of the host and the occurrence rate and mass of planets (Laughlin et al. 2004; Ida & Lin 2005), so that low-mass stars should have a much lower frequency of Jupiter-mass companions, while low-mass planets (Neptune-like and terrestrial-type) around these stars should be relatively common. Note, however, that if the disk initial conditions are independent of stellar mass, then opposite conclusions are reached (Kornet et al. 2006). Observational evidence so far collected by dedicated Doppler surveys of a few hundred bright M dwarfs (Butler et al. 2004; Rivera et al. 2005; Bonfils et al. 2005; Endl et al. 2006) appears to support the former scenario. Alternatively, both large-separation gas giants as well as “super-Earths” formed via the disk instability mechanism (e.g., Durisen et al. 2007, and references therein) might be found around low-mass stars (Boss 2006a,b). In this scenario, the inner (hot) super-Earths found by Doppler surveys (Rivera et al. 2005; Udry et al. 2007; Mayor et al. 2008; Forveille et al. 2008) would still have formed by collisional accumulation, while the outer (cold) super-Earths found by microlensing surveys (e.g., Beaulieu et al. 2006; Bennett et al. 2008) would have formed by disk instability followed by photoevaporative stripping of their gaseous envelopes by EUV/FUV radiation from nearby massive stars (Boss 2006b). The prediction of theoretical models that around massive stars planets might be more common, and more massive, is presently being investigated by dedicated surveys of Hertzsprung gap sub-giants (Johnson et al. 2006), heavily evolved stellar samples belonging to the red-giant branch and clump regions of the H-R diagram (Frink et al. 2002; Sato et al. 2003; Setiawan et al. 2003; Hatzes et al. 2005; Lovis & Mayor 2007; Niedzielski et al. 2007, and references therein) and early-type dwarfs (Galland et al. 2005).

The other important relationship uncovered so far between planet characteristics and frequencies and host properties is quantified by the strong dependence of planet occurrence rates on stellar metallicity. The observational evidence (Gonzalez 1997; Santos et al. 2004; Fischer & Valenti 2005) has found theoretical support within the context of the core accretion model (Ida & Lin 2004; Kornet et al. 2005). As increased surface density of solids would facilitate the growth of embryonic cores, and as stellar metallicity is naturally thought of as a proxy for the actual heavy metal content of the primordial circumstellar disk, then gas giant planet formation is greatly enhanced around more metal-rich stars. The alternative view of gas giant formation by local gravitational instability, instead, is less sensitive to the disk metal content, and as a consequence giant planets formed via this mechanism should be found orbiting metal-rich and metal-poor stars with roughly equal probability (Boss 2002). However, Mayer et al. (2007) have found that higher metallicity may encourage giant planet formation by disk instability because an increased mean molecular weight leads to lower gas pressure. The observed trend for $[\text{Fe}/\text{H}] \gtrsim 0.0$ is usually taken as strong support for the core accretion model, though recently evidence has emerged from surveys of giant stars (Pasquini et al. 2007) that the metallicity correlation is due at least in part to pollution of the surface layers of dwarf stars by ingested planetary materials. Doppler surveys biased toward high-metallicity stellar samples (Fischer et al. 2005; Bouchy et al. 2005) have begun in recent years, prompted by the enhanced chances of finding large numbers of planets. In order to better characterize the dependence of giant planet frequency in the metal-poor regime, two surveys have started monitoring stellar samples with $[\text{Fe}/\text{H}] \lesssim -0.5$. A southern sample of ~ 100 stars is being observed by the Geneva team (Mayor et al. 2003, <http://www.eso.org/observing/proposals/gto79/harps/4.txt>), while our group (Sozzetti et al. 2006, S06 hereafter) has focused on a northern sample ($\delta \gtrsim -25^\circ$) of ~ 200 objects.

In S06 we described our dedicated Doppler survey of metal-poor dwarfs with HIRES on Keck 1, and presented an assessment of the overall quality of our measurements, making use of the results for stars that showed no velocity variations. Here we report on results for all stars observed with Keck/HIRES to date. The structure of our second paper is the following. Sect. 2 provides a brief overview of the Keck/HIRES Doppler survey for giant planets orbiting low-metallicity main-sequence stars. We present in § 3 results for all the stars observed in our program. Sect. 4 is dedicated to a statistical analysis of all the data, to assess variability thresholds and the presence of linear and non-linear trends on a star-by-star basis. In § 5 we place quantitative limits on the detectable companion mass as a function of orbital period. Finally, in § 6 we discuss our results, and their implications for the frequency of gas giant planets in the metal-poor regime and for the observed correlation between stellar metallicity and planet occurrence; we compare our findings to the predictions of proposed models of giant planet formation, and we suggest venues to further our overall

understanding of this fundamental issue of planetary system science.

2. The Keck/HIRES Doppler survey of metal-poor dwarfs

2.1. Target sample

Table 1 lists 160 metal-deficient stars observed at least twice during our three-year long observing campaign. The list of targets includes spectral type, visual magnitude V , effective temperature T_{eff} , metallicity $[\text{Fe}/\text{H}]$, stellar mass M_{\star} , $B - V$ and $V - K$ colors, surface gravity $\log g$, and distance estimate d (based on their *Hipparcos* parallax when available, photometric otherwise). The complete list included 200 stars, but for 20% of the sample the non-optimal timing of the observing nights at Keck did not allow us to collect multiple exposures before the program was ended. About 10% of the targets in Table 1 are also in the list of southern metal-poor stars observed with HARPS, and a similar fraction has also been observed by the California team (with about 50% of these subsamples appearing in the target lists of all three groups).

As described in S06, all stars are drawn from the Carney-Latham and Ryan samples of metal-poor, high-velocity field stars (e.g., Carney et al. 1994; Ryan 1989; Ryan & Norris 1991). Based on a decade-long radial-velocity monitoring with the CfA Digital Speedometers (Latham 1992) none of our program stars showed signs of velocity variation at the 0.5 to 1.0 km s⁻¹ level. Additional target selection criteria are driven by the need to find a balance between the sample size, the amount of observing time devoted to each target, and the achievability of a radial-velocity (RV) precision good enough for planet detection, and this ultimately imposed constraints on the properties of the target sample. In the end, based on detailed simulations with the CfA library of synthetic stellar spectra (see S06 for details), we selected targets with $V \lesssim 12$ mag, $T_{\text{eff}} \lesssim 6000$ K, and $-2.0 \lesssim [\text{Fe}/\text{H}] \lesssim -0.6$. Table 1 lists photometric temperatures and spectroscopic metallicities determined from comparison of observed and synthetic spectra, and stellar masses derived from comparison with the Yonsei-Yale stellar evolution models (Demarque et al. 2004) in a color-magnitude diagram (the best agreement over a wide range of $[\text{Fe}/\text{H}]$ values was obtained using the $V - K$ colors). The analysis closely follows the procedures of Carney et al. (1987, 1994). Notable changes with respect to that approach include the determination of photometric T_{eff} values using the Alonso et al. (1996) calibrations and the adoption of reddening values based on $uvby\beta$ photometry whenever possible instead of the default approach of using reddening maps from Burstein & Heiles (1982). All new details of the procedure as applied to all stars included in the proper motion survey of Carney et al. (1994) will be discussed extensively in a forthcoming paper (Carney et al., in preparation). As far as the subset of metal-poor stars

presented in Table 1 is concerned, typical uncertainties on T_{eff} , $[\text{Fe}/\text{H}]$, and M_{\star} are 100 K, 0.1 dex, and $0.1 M_{\odot}$ respectively. In order to verify the reliability of our internal errors on the stellar parameters we have carried out an independent check comparing our temperature, metallicity, and mass estimates with those reported in the SPOCS catalog (Valenti & Fischer 2005; Takeda et al. 2007) for the subset of 16 stars in common between our program and the one of the California team. The result of the comparison is shown in Figure 1. The agreement between the two sets of data is broad: A straight line fit in three cases gives slopes of 0.99, 1.05, and 0.89 for the top, center, and lower panel, respectively. The mean differences in the three parameters are -37 ± 33 K, 0.04 ± 0.03 dex, and $-0.002 \pm 0.016 M_{\odot}$, respectively, with standard deviations of 134 K, 0.12 dex, and $0.06 M_{\odot}$, respectively. Although based on a relatively small subset of common stars, these findings indicate that our values are compatible with those reported in the SPOCS catalog within our quoted errors, reinforcing our confidence on the reliability of the procedures we adopted to determine the stellar parameters and related uncertainties for our program stars. Updated estimates of the stellar parameters and detailed spectroscopic abundance determinations for this sample (e.g., including $[\text{Fe}/\text{H}]$ and $[\alpha/\text{Fe}]$), based on our high-resolution, high- S/N Keck spectra, will be the main focus of future work.

2.2. Observations

All observations were collected with HIRES and its I_2 cell (except for one Iodine-free template exposure per target) on the Keck 1 telescope (Vogt et al. 1994). The spectrometer slit used at Keck was $0.57''$. During the observing runs in 2003 and 2004, with the old HIRES CCD setup the nominal resolving power and spectral coverage were $\sim 65,000$ and $3850\text{-}6200 \text{ \AA}$, respectively. These figures, after the summer 2004 upgrade of the HIRES CCD, became $\sim 71,000$ and $3200\text{-}8800 \text{ \AA}$, respectively. As described in S06, exposure times were calculated on a star by star basis, with the aim of reaching uniform RV precision ($\approx 10 \text{ m s}^{-1}$) for the whole sample. The resulting average exposure time, yielding a typical S/N ratio of $\sim 100 \text{ pixel}^{-1}$, is 9 min. Integration times were limited to a maximum of 15 minutes, in order to minimize timing uncertainties and subsequent systematic errors in the barycentric velocity correction.

2.3. Analysis

To extract the RV information from each star+iodine spectrum, we perform a full spectral modeling which includes the reconstruction of the asymmetries, spatial and temporal

variations in the HIRES instrumental profile at the time of observation. First, the spectrum is subdivided into smaller segments, and then for each segment a multi-parameter, χ^2 -minimization scheme is performed and a best-fit model is obtained, based on a template (iodine-free) spectrum of the target and a laboratory spectrum of the I₂ cell (e.g., Valenti et al. 1995; Butler et al. 1996). The RV of the target is measured with respect to the template, while the superimposed I₂ lines provide the wavelength calibration information. Uncertainties in the RV measurements are determined from the scatter about the mean for each spectral order divided by the square root of the number of orders containing I₂ lines. Our algorithm for precision RV measurements follows a procedure based on the methodology developed for the AFOE spectrograph (Korzennik et al. 2000), and adapted for the processing of HIRES spectra, as described in Sozzetti et al. (2008).

3. Radial-velocity results

We summarize in Table 2 our radial-velocity results by giving, for each star, the number of observations, the total rms RV scatter, the mean internal uncertainty, and the duration of monitoring. All radial velocities not presented in this work are available upon request from A. Sozzetti.

As discussed in S06, the average RV scatter of the whole sample is $\bar{\sigma}_{\text{rms}} \simeq 9 \text{ m s}^{-1}$. No statistically significant trends of σ_{rms} with V , T_{eff} , or $[\text{Fe}/\text{H}]$ are present in the data, an indication that our predicted exposure times based on simulations with the CfA library of synthetic stellar spectra were reliable. Inspection of Table 2 shows that, while most of the objects in the sample have RV scatter comparable to the internal error estimates, several stars exhibit σ_{rms} larger (in some cases, much larger) than σ_{int} . It is then necessary to perform a thorough statistical examination of the complete RV dataset, testing for variability and long-term trends (given the limited and typically very sparse number of spectra per star, a search for significant periodic signals is not feasible).

3.1. Statistical Analysis: Testing for excess variability

Almost all stars in our sample belong to the halo or thick-disk populations (Carney et al. 1994, 1996). In particular, population membership probabilities calculated following the methods described in Bensby et al. (2003), Venn et al. (2004), and Reddy et al. (2006) indicate that 87% of the stars observed in the Keck/HIRES survey (138 out of 160) have less than 20% chances of belonging to the thin disk of the Milky Way. The fact that these stars

are likely members of the thick-disk and halo populations also implies that they typically have very old ages (e.g., Holmberg et al. 2007). An advantage of dealing with rather old main-sequence stars is that they tend to be slow rotators (all our program stars have projected rotational velocities $v \sin i \leq 10 \text{ km s}^{-1}$), and exhibit low levels of chromospheric emission. Both rotation and stellar activity constitute sources of intrinsic radial velocity jitter that can mask, and sometimes even mimic, the presence of orbital reflex motion due to planetary mass companions (Saar et al. 1998; Santos et al. 2000; Queloz et al. 2001; Paulson et al. 2004), particularly in the case of young (e.g., Setiawan et al. 2008; Huélamo et al. 2008) and evolved (e.g., Carney et al. 2003, 2008a, 2008b; Hekker et al. 2008) stars. For the targets observed in our survey, sources of intrinsic RV variability should then be minimal. For this reason, we did not add in quadrature to the internal error estimates any terms representing intrinsic stellar variability. We then ask if the scatter σ_{rms} in the velocities is consistent with our σ_{int} estimate for each star. We perform three tests.

First, we perform an F -test, comparing the ratio of variances $\sigma_{\text{rms}}^2/\sigma_{\text{int}}^2$. Next, we use the distribution of the reduced χ_ν^2 (with $\nu = N - m$ being the number of degrees of freedom, and $m = 1$ for a constant model) to test if the velocities are consistent with being drawn from a normal distribution with variance σ_{int}^2 . Finally, we determine whether the underlying one-dimensional probability distributions of σ_{rms} and σ_{int} are significantly different, based on Kuiper’s Ku test. This test is preferable to the more widely known Kolmogorov-Smirnov ($K - S$) test, as while both tests determine the maximum deviation between two cumulative distribution functions, the former is equally sensitive in the tails as at the median. This test is carried out only for objects with $N > 3$, as for very small datasets it is not meaningful. In all cases, excess variability in the dataset for any given star can be assessed, in a statistical sense, when a small value of the false alarm probability ($\text{Pr}(F)$, $\text{Pr}(\chi_\nu^2)$, and $\text{Pr}(Ku)$, respectively) indicates that the null hypothesis should be rejected (at a given confidence level). Given the relatively small number of observations per target, to account for the possibility of outliers in the data, and to minimize the likelihood of obtaining more than 1 false signal in our sample, we have decided to adopt high thresholds of the false-alarm probabilities ($Pr < 0.005$, i.e. a 99.5% confidence level) and to request stringent agreement between the three tests, before any given object can be flagged as very likely variable.

We report in Table 3 the results of the variability tests applied to the entire sample. Nine stars, with as few as 3 and as many as 11 observations, are identified as variables based on the above criteria. These nine objects (HD 7424, G197-45, G 237-84, G 63-5, G 135-46, HD 192718, HD 210295, G 27-44, and G 28-43) all exhibit $\sigma_{\text{rms}}/\bar{\sigma}_{\text{int}} \gtrsim 4$, i.e. a scatter in the measurements at least four times larger than the nominal average internal error. Ten stars are recognized as significantly variable by two out of three tests, and these comprise objects with $2.0 \lesssim \sigma_{\text{rms}}/\bar{\sigma}_{\text{int}} \lesssim 3.0$. Twenty two stars fail only one test, and for the remaining 119

objects all tests return $Pr > 0.005$. All radial velocities for stars not deemed significantly variable, i.e. corresponding to objects with $\sigma_{\text{rms}}/\bar{\sigma}_{\text{int}} \lesssim 3.0$, are presented in Table 5.

3.2. Long-term linear and curved trends: Individual objects

We next investigate the possibility that the RV data for each object can be better described by a linear slope, which would indicate the presence of a massive, distant companion orbiting with a period greatly exceeding the duration of the observations ($\gg 3$ yr). Such long-term trends could in fact directly affect our search for planetary-mass companions with $P < 3$ yr, and thus should be immediately subtracted if present.

For each star with at least three RV observations, we fit a straight line to the measured velocities. We derive a best-fit slope and its uncertainty, then verify its significance using an F -test that compares the weighted sum of the squares of the residuals from the straight line fit to that about the mean. Large values of F (and correspondingly low values of $P(F)$) would indicate that the data are better described by a straight line, i.e. they display a significant long-term linear trend. For the purpose of this study, we use again the prescription ($Pr(F) < 0.005$) to discriminate between statistically significant and insignificant slopes. We conclude by re-computing $\sigma_{\text{rms}}/\bar{\sigma}_{\text{int}}$ and $Pr(\chi^2_\nu)$ on the post-fit residuals, to determine whether the two-parameter model can or cannot be considered satisfactory (even in cases when a significant slope is found). The results are summarized in Table 4.

For most stars, insignificant slopes are derived. For six of the nine stars that were flagged as clearly variable in the previous section ($\sigma_{\text{rms}}/\bar{\sigma}_{\text{int}} \gtrsim 4$), the slope is quite significant, and after subtraction of the linear RV trends the post-fit residuals agree much more closely with the measurement errors. We show the best-fit linear trends for these objects (HD7424, G197-45, G237-84, G63-5, G135-46, HD192718) in Figure 2. We discuss the results for these stars collectively below. As for the other three variables (HD210295, G27-44, and G28-43), the RV residuals are not significantly improved after fitting for a linear trend. We show in Figure 3 the RVs collected for the three stars. They all clearly exhibit significantly non-linear RV variations. The results for each of these stars are discussed separately below.

None of the 32 stars which fail either one or two of the three statistical tests for variability appears to exhibit significant ($Pr(F) < 0.005$) long-term trends. However, a significant slope is found for one of the stars (G204-30) which do not appear as RV variables based on all tests. The results for this object are also discussed below.

3.2.1. Stars with secular trends

The seven stars with significant long-term linear slopes (HD 7424, G 197-45, G 237-84, G 63-5, G 135-46, HD 192718, and G 204-30) are all unevolved dwarfs with $-1.0 \lesssim [\text{Fe}/\text{H}] \lesssim -0.6$ (see Table 1). In the five cases that are bright enough to have been observed by *Hipparcos*, the single-star astrometric solutions show no indication of excess scatter, suggesting the RV trends we see are likely due to a brown-dwarf or stellar companion in a very long-period orbit. One of these, G 63-5, is listed in the Washington Double Star Catalog as having a common proper motion M0 binary companion at $\sim 80''$, but this is likely to be too distant to be the cause of the observed slope (at a distance $d \sim 60$ pc, this corresponds to a linear orbital semi-major axis of ~ 5000 AU). All radial velocities collected for these objects are presented in Table 6.

3.2.2. G 27-44

This relatively metal-poor ($[\text{Fe}/\text{H}] \simeq -0.80$) dwarf was observed by *Hipparcos*, which did not detect any significant deviations from a single-star astrometric model. The object was included in the *I*-band CCD imaging search for wide metal-poor binaries of Zapatero Osorio & Martín (2004), who searched for companions within $\sim 25''$ of 473 metal-deficient stars. This survey was sensitive to nearby companions up to 5 mag fainter than the target star. No indication of companions within the survey limits was found. We conclude this star is orbited by a previously undetected brown dwarf or stellar companion. The RV data collected for G 27-44 are presented in Table 7. Direct imaging observations in the infrared are ongoing to ascertain its nature.

3.2.3. G 28-43

This low-metallicity ($[\text{Fe}/\text{H}] \simeq -1.80$) dwarf was observed by *Hipparcos*, but it is an apparent case of misidentification. The entry HIP 114349 includes the components CCDM J23096+0043 A and CCDM J23096+0043 B. The secondary (CCDM J23096+0043 B, $V = 11.5$) is supposedly placed at $12.2''$ from the primary, at a position angle of 195 deg. However, Zapatero Osorio & Martín (2004) do not confirm it using their data and images from the Digitized Sky Surveys. On the other hand, Woolf & Wallerstein (2005) argue that G 28-43 seems to be a double-lined spectroscopic binary. The presence in the spectrum of light from a close-in massive companion (with a separation $< 1'' - 2''$ would in fact explain the large error bars we obtain for the radial velocities (presented in Table 7). This star thus appears

to be orbited by a previously undetected brown dwarf or stellar companion. Direct imaging observations in the infrared are ongoing to ascertain its nature.

3.2.4. *HD 210295*

This low-metallicity star ($[\text{Fe}/\text{H}] \simeq -1.50$) star was observed by *Hipparcos*, which did not detect any significant deviations from a single-star model. Again, Zapatero Osorio & Martìn (2004) do not find evidence for companions up to 5 mag fainter within $\sim 25''$. The RV data collected for HD 210295 are presented in Table 7. On the one hand, they appear compatible with the existence of a short-period companion inducing a relatively low velocity semi-amplitude ($\approx 50 - 60 \text{ m s}^{-1}$). On the other hand, HD 210295 is the most evolved among the stars included in our survey. Hekker et al. (2008) have recently presented results from a multi-year precision RV monitoring campaign of ~ 180 K giants. They find a very significant inverse correlation between surface gravity and random RV ‘jitter’, as well as a large number of stars with correlated, periodic RV variations that do not correlate with surface gravity. In particular, stars with $\log g \approx 2.8 - 3.0$, similar to HD 210295, often exhibit random half peak-to-peak RV variations of about $\sim 50 - 60 \text{ m s}^{-1}$. Based on this evidence, it appears likely that the RV variations for HD 210295 are of intrinsic nature, but we strongly encourage additional RV observations to better understand whether the RV jitter is clearly random or if it can be modeled with a periodic component.

3.2.5. *Summary*

Overall, our results indicate that none of the stars with clearly detected RV variations appear to be orbited by massive giant planet companions with periods shorter than the survey duration. Most of the variable stars exhibit long-term trends compatible with the existence of very distant brown dwarf or stellar companions. The only clear candidate exhibiting short-term, low-amplitude velocity variability is an evolved star, and the more likely explanation for the observed RV variability is to be found in some type of mechanism intrinsic to the star. Given the limited amount of data collected (typically, only a handful of observations per star over a time-span of three years), we can say very little about companions inducing RV variations close to the average internal errors we obtain ($\simeq 10 \text{ m s}^{-1}$).

4. Limits on companion mass and period

The quantitative determination of the sensitivity of an RV survey such as ours to planetary companions of given mass and period relies upon detailed numerical simulations of synthetic datasets of RV observations of a population of planetary systems of varying orbital properties and masses. The ability to recover, with a given level of statistical significance, the presence of a planetary signal or not translates into lower limits on the detectable (minimum) companion mass as a function of e.g. period and eccentricity (for an assumed mass of the central star).

4.1. Methodology

Limits on companion detectability for a number of RV planet surveys have been presented in the past by, e.g., Walker et al. (1995), Cumming et al. (1999, 2008), and Endl et al. (2002, 2006). Nelson & Angel (1998), Eisner & Kulkarni (2001), Cumming (2004), and Narayan et al. (2005) have derived analytical expression for the detectability of a given RV signal in a variety of situations (large/small number of observations, periods shorter/longer than the duration of the observations, small and large companion masses). They used two different approaches, one based on a periodogram analysis to identify significant periodicities in a dataset, the other based on χ^2 - and F -tests to detect excess residuals above an assumed level of Gaussian noise.

For our project, the periodogram approach is not feasible, due to the combined effect of very poor sampling and small number of observations per star. Thus, we rely on the alternate statistical approach. We start from the null hypothesis that there is no planet, i.e. that the RV of a given star is constant, and that the observed scatter is only due to measurement uncertainties. For each star in our program, we then add Keplerian signals to the data, at the exact times of observation, and perform a χ^2 -test with a 99.5% confidence level (to minimize the number of false positives, given the sample size) on the new set of velocities, to verify if they are still consistent with being drawn from a Gaussian distribution with variance $\bar{\sigma}_{\text{int}}$. Suppose χ_0^2 is the value provided by the null model (no planet), then the test fails when $Pr(\chi^2 \geq \chi_0^2) \leq 0.005$. In this case, the planet is considered detected. We employed the χ^2 -test to analyze 8×10^6 star+planet systems, with the orbital elements and mass of the perturbing companion in the following ranges: $0.01 \leq P \leq 20$ yr, $0.0 \leq e \leq 1.0$, $0.0 \leq i \leq \pi/2$, $0.0 \leq \omega \leq 2\pi$, $0.0 \leq \tau \leq P$, $0.1 \leq M_c \leq 20 M_J$. To transform any detected RV amplitude K (in m s^{-1}) into a corresponding minimum companion mass (in M_J), we use the formula:

$$M_c \sin i = \frac{K}{28.4 \text{ m s}^{-1}} \left(\frac{M_\star}{M_\odot} \right)^{2/3} \left(\frac{P}{\text{yr}} \right)^{1/3} \sqrt{1 - e^2} \quad (1)$$

In the simulations, the average stellar mass for our sample was utilized, i.e. $M_\star = 0.80 M_\odot$.

4.2. Limits on companions and survey completeness

Figure 4 displays the survey sensitivity determined by this method in the $M_p \sin i - P$ plane. The limits shown in the figure are for 50% and 95% survey completeness, and for three realizations with different values of eccentricity: perfectly circular orbits, $e = 0.3$, corresponding to the median value of the e distribution of known exoplanets, and $e = 0.8$, which virtually encompasses the whole extrasolar planet sample. Note that the mass limits for the planets are somewhat conservative, because for less massive stars these companion mass values would be lower.

The results shown in Figure 4 indicate that we would have detected virtually all companions on circular orbits with $M_c \sin i \gtrsim 3.0(P/1 \text{ yr})^{1/3} M_J$, and orbital periods $P \lesssim T$, with $T \approx 3 \text{ yr}$ being the average timespan of the observations. In this period range, the corresponding value of radial-velocity amplitude for secure detection is $K \approx 100 \text{ m s}^{-1}$, or $K/\sigma_{\text{rms}} \simeq 10$, if we use as a proxy for the average RV uncertainty of our data the median RV scatter of the whole sample $\sigma_{\text{rms}} \simeq 9 \text{ m s}^{-1}$. Instead, an amplitude such that $K/\sigma_{\text{rms}} \simeq 3$ for $P < T$ (corresponding to $M_c \sin i \gtrsim 1.0(P/1 \text{ yr})^{1/3} M_J$), is recovered only 50% of the time. Both results are in close agreement with those reported by e.g. Cumming (2004).

Windows of poor detectability in period occur for two main reasons, i.e. due to the data structure (number of observations and phase coverage) and to the 1-yr seasonal period which affects any ground-based observing program. At these periods, the minimum detectable mass is anywhere between a factor of 1.5 (in the former case) and an order magnitude (in the latter case) larger.

Orbital eccentricity has a very significant impact on the detection efficiency, as during the survey critical orbital phases of eccentric orbits can be missed due to sparse sampling, and a star with a very eccentric companion may show no appreciable RV variations. This effect is not prominent for mild eccentricities, up to values of e close to the median of the exoplanet sample known to-date ($e = 0.3$). For very eccentric orbits (the case $e = 0.8$ is shown in Figure 4), a much larger signal is required for secure detection. The equivalent sensitivity in mass degrades by a factor of a few.

For periods exceeding the time baseline of the observations ($P > T$), detection sensitivity drops quickly due to the fact that observations cover only a portion of an orbit. This is a well-known result, discussed by many groups in the past that addressed the issue of planet detection sensitivity both in the context of Doppler (see references at the beginning of this section) as well as astrometric (for a review, see Sozzetti 2005, and references therein) surveys for planets. For comparison, we show in Figure 5, as a function of P , the minimum RV amplitude K_{\min} for 50% and 95% detection probability (dashed lines) obtained in the simulations superposed on the analytical results (solid thick lines) of Cumming (2004). In particular, the predicted behavior $K_{\min} \propto P$ for $P > T$ for the 50% detection curve is very closely followed. For the case of 95% completeness, we find a best-fit behavior $K_{\min} \propto P^{3/2}$, and for 99% completeness (not shown) we correctly recover the steeper $K_{\min} \propto P^2$ behavior obtained by Cumming (2004).

Based on the results of this and the previous section, we conclude that none of the metal-poor stars surveyed in our program reveal an excess RV scatter attributable to Keplerian reflex motion caused by a Jovian-mass companion with $P < T$.

4.3. Frequency of close-in sub-stellar companions

With this null result in hand, it is possible to draw conclusions on the frequency of giant planets orbiting metal-poor dwarfs to which our survey is sensitive (95% completeness for $K > 100 \text{ m s}^{-1}$, $P < 3 \text{ yr}$, and $e < 0.3$). Given the relatively limited sample size, we elect to follow the approach described in e.g. Burgasser et al. (2003) and McCarthy & Zuckermann (2004), rather than the more common procedure based on Poisson uncertainties. We then use the binomial probability distribution, which determines the probability $P(f_p; n, N)$ of n detections given a sample of size N when the true planetary companion frequency is f_p as:

$$P(f_p; n, N) = \frac{N!}{n!(N-n)!} f_p^n (1-f_p)^{N-n} \quad (2)$$

The probability distribution is not symmetric about its maximum, thus we report the range in f_p that delimits 68% of the integrated probability function, equivalent to $1-\sigma$ limits for a Gaussian distribution. We make two assumptions. First, based on the null result presented above, we set $n = 0$ and $N = 160$ (Figure 6, top panel), and find $f_p = 0.24_{-0.24}^{+0.43}\%$. Thus, at the $1-\sigma$ confidence level, we constrain the frequency of giant planets orbiting metal-poor stars to be $f_p < 0.67\%$. If we make the hypothesis that indeed we missed one planet with $K > 100 \text{ m s}^{-1}$ and $P < 3 \text{ yr}$, $e < 0.3$, then $n = 1$, and we find that there is a 68% chance of f_p ranging between 0.44% and 2.0%, thus $f_p = 0.62_{-0.18}^{+1.38}\%$.

5. Summary, discussion and conclusions

We have presented an analysis of three years of precision Doppler measurements of 160 metal-poor stars from our Keck/HIRES radial-velocity survey.

We have performed several statistical tests for excess variability and long-term trends. Our sample contains nine clear RV variable stars (identified on the basis of the accordance between different statistical indicators). Six of them exhibit significant long-term linear trends, indicative of companions in the stellar/sub-stellar mass regime on very long periods (P much larger than the survey duration T). After subtraction of these long-term trends, the RV residuals are consistent with our measurement errors. This sample is currently the subject of a direct imaging search in the IR to better characterize the actual nature of the detected companions, whose results will be reported in a forthcoming paper. As for the remaining three stars which appear to be RV variables, their non-linear RV variations are again compatible with the presence of long-period massive sub-stellar or stellar companions, or due to some type of mechanism intrinsic to the star. Given the limited amount of data collected (typically, only a handful of observations per star over a time-span of three years), we can say very little about companions inducing RV variations close to the average internal errors we obtain ($\simeq 10 \text{ m s}^{-1}$). Overall, our results indicate that none of the stars with clearly detected RV variations appear to be orbited by massive giant planet companions with periods shorter than the survey duration.

Based on our RV data and numerical simulations of planetary signatures, we have placed quantitative lower-mass limits for sub-stellar companions orbiting our metal-poor sample, as a function of orbital separation. Our survey would have detected, with a 99.5% confidence level, virtually all companions on low-eccentricity orbits ($e < 0.3$) with velocity semi-amplitude $K \gtrsim 100 \text{ m s}^{-1}$, or $M_c \sin i \gtrsim 3.0 M_J (P/\text{yr})^{(1/3)}$, and orbital periods $P \lesssim 3 \text{ yr}$. None of the stars in our sample exhibits radial-velocity variations compatible with the presence of companions inducing $K > 100 \text{ m s}^{-1}$ and with periods shorter than the survey duration. The observed dearth of gas giant planets within 2 AU of metal-poor stars ($-2.0 < [\text{Fe}/\text{H}] < -0.6$), allows us to confirm and extend previous findings (e.g., Santos et al. 2004; Fischer & Valenti 2005). The resulting average frequency of gas giants orbiting metal-poor dwarfs with $-2.0 \lesssim [\text{Fe}/\text{H}] \lesssim -0.6$ is $f_p < 0.67\%$ (at the $1 - \sigma$ level). We note that our null result also provides supporting evidence for the existence of a ‘brown dwarf desert’ (e.g.,) which extends to low metallicity stars. Indeed, current estimates from ongoing Doppler surveys imply a frequency $f_{\text{BD}} = 0.5 \pm 0.2\%$ of close-in ($a \leq 3 \text{ AU}$) brown-dwarf companions to solar-type stars with $[\text{Fe}/\text{H}] \gtrsim 0.0$ (see for example Marcy et al. 2005). However, whether f_{BD} correlates with stellar metallicity, depending on the range of orbital separations considered, is presently a still poorly understood issue, and we will address this

point in detail in a forthcoming paper which will describe the results of our IR imaging search for companions around metal-poor stars with RV trends.

We are now in a position to put the null result from our Doppler survey in the context of the observed correlation between the rate of occurrence f_p of giant planets and the metallicity of their main-sequence solar-type stellar hosts. The fact that metal-rich stars have a higher probability of harboring a giant planet than their low-metallicity counterparts has been quantified in particular by Santos et al. (2004) and Fischer & Valenti (2005) (for a review of the issue, see for example Udry & Santos 2007). Using all the available data at that time, with no selection criteria based on orbital period, RV amplitude, planet mass, and metallicity, Santos et al. (2004) found that $f_p \propto [\text{Fe}/\text{H}]$ for metallicities above solar, while $f_p \sim \text{const.}$ for metallicities below solar. Fischer & Valenti (2005) constructed a sample of stars from their Doppler survey with uniform detectability threshold ($K > 30 \text{ m s}^{-1}$, $P < 4 \text{ yr}$), and found an even steeper dependence of f_p on $[\text{Fe}/\text{H}]$, fitting a power-law $f_p = 0.03 \times 10^{2.0[\text{Fe}/\text{H}]}$ in the metallicity range $-0.5 < [\text{Fe}/\text{H}] < 0.5$. Both analyses concluded that at least 25% of the stars with twice the metal content of our Sun ($[\text{Fe}/\text{H}] = 0.3$) are orbited by a giant planet ($M_p \gtrsim 1 M_J$), and this number decreases to below 5% for solar-neighborhood dwarfs with $[\text{Fe}/\text{H}] \lesssim 0.0$.

We have combined our dataset with the uniform sample of Fischer & Valenti (2005), taking care to select objects from the latter sample with planets that would have been detected by both surveys, i.e. with $K > 100 \text{ m s}^{-1}$ and $P < 3 \text{ yr}$. In Figure 7 we present the fraction of planet-hosting stars as function of $[\text{Fe}/\text{H}]$ for the combined sample. The ratio of planet-bearing stars to all stars is labeled above each 0.5-dex bin in metallicity. Error bars for $[\text{Fe}/\text{H}] > -1.0$ are calculated assuming Poisson statistics (i.e., the percentage of stars with planets divided by the square root of the number of planets), while, given the small-number statistics, a binomial distribution is utilized to determine the $1 - \sigma$ error bars for $[\text{Fe}/\text{H}] < -1.0$. In the bin $-1.0 < [\text{Fe}/\text{H}] < -0.5$ the merging of the two datasets provides for a five-fold increase in the number of stars surveyed with respect to the analogous analysis reported in Figure 4 of Fischer & Valenti (2005). Overall, the probability of forming gas giant planets with $K > 100 \text{ m s}^{-1}$ and $P < 3 \text{ yr}$ around metal-poor stars ($[\text{Fe}/\text{H}] < 0.0$) appears suppressed by a factor of several with respect to that of finding any around metal-rich stars ($[\text{Fe}/\text{H}] > 0.0$).

To investigate this correlation in more detail, we divide the stars into finer 0.25-dex metallicity bins, and limit ourselves to the metallicity range $-1.0 < [\text{Fe}/\text{H}] < 0.5$, for which better statistics are available. Figure 8 shows a smooth increase in the fraction of stars with planets as a function of increasing metallicity above $[\text{Fe}/\text{H}] = 0.0$, and an approximately constant detection rate for metallicity below solar. About 7.5% of stars with $[\text{Fe}/\text{H}] \simeq 0.3$

host planets with $K > 100 \text{ m s}^{-1}$ and $P < 3 \text{ yr}$, but $f_p \sim 1.0\%$ for companions with the same characteristics orbiting sub-solar metallicity stars. The two curves quantify the f_p –[Fe/H] relationship in terms of a power-law with the same index as the Fischer & Valenti (2005) functional form, with and without a constant term:

$$f_p(\%) = 1.3 \times 10^{2.0[\text{Fe}/\text{H}]}(+0.5) \quad (3)$$

We confirm that the likelihood of a star to harbor a planet more massive than Jupiter within 2 AU is a steeply rising function of the host’s metal content. However, while $f_p(-1.0 < [\text{Fe}/\text{H}] < -0.5)$ appears to be a factor of several lower than $f_p([\text{Fe}/\text{H}] > 0.0)$, it is indistinguishable from $f_p(-0.5 < [\text{Fe}/\text{H}] < 0.0)$. Overall, the data for stars with $-1.0 \lesssim [\text{Fe}/\text{H}] \lesssim 0.0$ are compatible, in a statistical sense, with a constant occurrence rate $f_p \simeq 1\%$, as the two power-law fits are statistically indistinguishable one from the other. The difficulty in representing the f_p –[Fe/H] relationship as a single power-law for the entire range of metallicities encompassed in this analysis might either indicate bi-modality in the distribution (flat behavior for $[\text{Fe}/\text{H}] < 0.0$ plus strong rise for $[\text{Fe}/\text{H}] > 0.0$), or simply constitute an as of yet not well-characterized low-metallicity tail. Similar conclusions are derived by Udry & Santos (2007), who analyzed the average f_p –[Fe/H] in the California-Carnegie and Geneva samples. Our results can usefully inform theoretical studies of the process of giant planet formation across two orders of magnitude in metallicity. We summarize below the existing predictions, and then discuss how our data can contribute to test them.

Core accretion models for giant planet formation are today mature enough to make clear predictions concerning the mass-range, orbital period distribution, and frequency of planets orbiting stars of varying metallicity (assuming their metal content closely track the metallicity of the protoplanetary disk in which they formed). In the standard model of gas giant planet formation by core accretion (e.g., Pollack et al. 1996; Alibert et al. 2005), several studies have highlighted how f_p (integrated over a wide range of planetary masses) should be a monotonically decreasing function of decreasing [Fe/H] (e.g., Ida & Lin 2004; Kornet et al. 2005; Matsuo et al. 2007). Indeed, Matsuo et al. (2007) propose that there should be an effective low-metallicity limit at $[\text{Fe}/\text{H}] \approx -1.0$ below which giant planets cannot form by core accretion at all. Those authors also suggest the existence of a metallicity dependent upper mass limit, of about $2 M_J$ at $[\text{Fe}/\text{H}] \approx -1.0$. On the other hand, the likelihood of finding Neptune-mass planets might not correlate strongly with [Fe/H] of the host (Ida & Lin 2004; Benz et al. 2006). Finally, short-period planets may not be found around metal-poor stars either because of an inverse metallicity-dependence of migration rates (Livio & Pringle 2003) or due to longer timescales for giant planet formation around metal-poor stars, and thus reduced migration efficiency before the disk dissipates (Ida & Lin 2004). As for the

alternative scenario of giant planet formation by disk instability, the situation is less clear, even for the metallicity correlation (Boss 2002; Matsuo et al. 2007; cf. Mayer et al. 2007). Estimated masses for gas giant planets formed by disk instability range from Saturn-mass (Mayer et al. 2004; Boss 2008) to ~ 10 Jupiter masses (Boss 1998; Mayer et al. 2004). Other authors (Rice et al. 2003; Rafikov 2005) have concluded that giant planets formed by disk instability should populate preferably the high-mass tail of the mass distribution. Low migration efficiency in gravitationally unstable disks implies that planets formed by this mechanism should be found on wide orbits (Rice et al. 2003; Mayer et al. 2004; Rafikov 2005).

We do not detect any massive planets ($M_p \sin i \gtrsim 1 - 4 M_J$) within 2 AU of metal-poor stars with $-2.0 \lesssim [\text{Fe}/\text{H}] \lesssim -0.6$, and constrain their occurrence rate to be no larger than $f_p \simeq 1\%$. All long-period trends identified in our survey are compatible with being induced by brown dwarf or stellar companions. Based on the above expectations, these findings appear to be circumstantial evidence in favor of the core accretion mechanism of giant planet formation. On the other hand, the probability of a star with $-1.0 \lesssim [\text{Fe}/\text{H}] \lesssim 0.0$ to host a massive planet within 2 AU appears constant, and this could be read as supporting evidence for the alternative disk instability model. However, though very useful, our results are not resolute, and at least three observational avenues can be identified to expand and improve the statistics and thus further constrain proposed models.

First, it is necessary to improve on the mass sensitivity threshold of the surveys. The formation of lower-mass giant planets around relatively low-metallicity stars is not completely inhibited, as recently testified by the announcements of a giant planet ($M_p \sin i = 1.8 M_J$) orbiting HD 171028 ($[\text{Fe}/\text{H}] = -0.49$, Santos et al. 2007) at an orbital distance of ~ 1.3 AU ($K \simeq 60 \text{ m s}^{-1}$) and of a two-planet system ($M_p \sin i \simeq 0.9 M_J$ and $M_p \sin i \simeq 0.5 M_J$) around HD 155358 ($[\text{Fe}/\text{H}] = -0.65$, Cochran et al. 2007), with orbital radii between ~ 0.6 AU and ~ 1.3 AU ($K \simeq 40 \text{ m s}^{-1}$ and $K \simeq 15 \text{ m s}^{-1}$, respectively). None of these stars were included in our Keck survey either because of the $[\text{Fe}/\text{H}]$ cut-off, or due to other selection criteria (proper motion, declination limits) in the original Carney et al. (1994) and Ryan (1989) surveys from which our sample was drawn. However, the evidence for a few objects in our sample with apparently short-term rms RV variations exceeding 2 to 3 times the measurements uncertainties indicates that at lower masses the fraction of metal-poor stars hosting planets may be larger. Unfortunately, with our data we cannot confirm or rule out the early evidence for a vanishing $f_p - [\text{Fe}/\text{H}]$ correlation in the Saturn to Neptune companion mass regime, argued for by Udry & Santos (2007) and more recently corroborated by the findings of Sousa et al. (2008).

Second, studies of planet occurrence around metal-poor stars still suffer from small-

number statistics biases, and one would clearly gain further insight by expanding the sample size. Overall, only 200–300 objects are presently targeted from the ground in the metallicity regime $-2.0 \lesssim [\text{Fe}/\text{H}] \lesssim -0.5$, and when statistical analyses such as ours are carried out, usually only several tens of stars end up populating a given metallicity bin. In particular, at the present time we still cannot completely rule out the possibility that the evidence for bimodality in the metallicity distribution is simply due to the limited number of stars surveyed.

Finally, it would be very beneficial to extend the time baseline of the surveys, to probe the existence of longer period planets. This is the only way to assess the relative role of metallicity in migration processes, as different conclusions would be drawn in the event massive planets are found or not at orbital radii of several AUs.

While challenging, the above experiments may be successfully carried out by ongoing RV programs (e.g., Santos et al. 2007), next-generation RV surveys (e.g., Ge et al. 2007), upcoming ultra-high precision transit surveys in space such as Kepler (Borucki et al. 2003), and future high-precision space-borne astrometric observatories such as Gaia (Casertano et al. 2008), SIM/SIM-Lite (Unwin et al. 2008). These data are crucially needed in order to better our understanding of the complex interplay between planet formation processes, migration scenarios, and several important characteristics of the protoplanetary disks, such as their metal content.

An anonymous referee provided useful and timely comments and suggestions which helped improve the paper. GT acknowledges partial support for this work from NASA Origins grant NNG04LG89G. AS gratefully acknowledges the Kepler mission for partial support under NASA Cooperative Agreement NCC 2-1390. JBL was supported for this work by NSF grant AST-0307340. The data presented herein were obtained at the W.M. Keck Observatory, which is operated as a scientific partnership among the California Institute of Technology, the University of California and the National Aeronautics and Space Administration. The Observatory was made possible by the generous financial support of the W.M. Keck Foundation. The authors wish to recognize and acknowledge the very significant cultural role and reverence that the summit of Mauna Kea has always had within the indigenous Hawaiian community. We are most fortunate to have the opportunity to conduct observations from this mountain. This research has made use of NASA’s Astrophysics Data System Abstract Service and of the SIMBAD database, operated at CDS, Strasbourg, France.

REFERENCES

- Alibert Y., Mordasini C., Benz W., 2004, *A&A*, 417, L25
- Alonso, A., Arribas, S., Martinez-Roger, C. 1996, *A&A*, 313, 873
- Baglin, A., et al. 2002, in *Radial and Nonradial Pulsations as Probes of Stellar Physics*, eds. C. Aerts, T. R. Bedding, & J. Christensen-Dalsgaard, *ASP Conf. Ser.*, 259, 626
- Beaulieu, J.-Ph., et al. 2006, *Nature*, 439, 437
- Bennett, D., et al. 2008, *ApJ*, 684, 663
- Bensby, T., Feltzing, S., & Lundström, I. 2003, *A&A*, 410, 527
- Benz, W., Mordasini, C., Alibert, Y., & Naef, D. 2006, in *Tenth Anniversary of 51 Peg-b: Status of and prospects for hot Jupiter studies*, ed. L. Arnold, F. Bouchy, & C. Moutou, 24
- Bond, I., et al., 2004, *ApJ*, 606, L155
- Bonfils, X., et al. 2005, *A&A*, 443, L15
- Borucki, W. J., et al. 2003, in *Future EUV/UV and Visible Space Astrophysics Missions and Instrumentation*, eds. J. C. Blades & O. H. W. Siegmund, *Proc. SPIE*, 4854, 129
- Boss, A. P. 1998, *ApJ*, 503, 923
- Boss, A. P. 2002, *ApJ*, 567, L149
- Boss, A. P. 2006a, *ApJ*, 643, 501
- Boss, A. P. 2006b, *ApJ*, 644, L79
- Boss, A. P. 2008, *ApJ*, 677, 607
- Bouchy, F., et al. 2005, *A&A*, 444, L15
- Burgasser, A. J., Kirkpatrick, J. D., Reid, I. N., Brown, M. E., Miskey, C. L., & Gizis, J. E. 2003, *ApJ*, 586, 512
- Burstein, D., & Heiles, C., 1982, *AJ*, 87, 1165
- Butler, R. P., Marcy, G. W., Williams, E., McCarthy, C., Dosanjuh, P., & Vogt, S. S. 1996, *PASP*, 108, 500

- Butler, R. P., Vogt, S. S., Marcy, G. W., Fischer, D. A., Wright, J. T., Henry, G. W., Laughlin, G., & Lissauer, J. J. 2004, *ApJ*, 617, 580
- Butler, R. P., et al. 2006, *ApJ*, 646, 505
- Carney, B. W., Laird, J. B., Latham, D. W., & Kurucz, R. L. 1987, *AJ*, 94, 1066
- Carney, B. W., Latham, D. W., Laird, J. B., & Aguilar, L. A. 1994, *AJ*, 107, 2240
- Carney, B. W., Laird, J. B., Latham, D. W., & Aguilar, L. A. 1996, *AJ*, 112, 668
- Carney, B. W., Latham, D. W., Stefanik, R. P., Laird, J. B., & Morse, J. A. 2003, *AJ*, 125, 293
- Carney, B. W., Latham, D. W., Stefanik, R. P., & Laird, J. B. 2008, *AJ*, 135, 196
- Carney, B. W., Gray, D. F., Yong, D., Latham, D. W., Manset, N., Zelman, R., & Laird, J. B. 2008b, *AJ*, 135, 892
- Casertano, S., Lattanzi, M. G., Sozzetti, A., Spagna, A., Jancart, S., Morbidelli, R., Panunzio, R., Pourbaix, D., & Queloz, D. 2008, *A&A*, 482, 699
- Charbonneau, D., Brown, T. M., Burrows, A., & Laughlin, G. 2007, in *Protostars and Planets V*, B. Reipurth, D. Jewitt, and K. Keil (eds.), University of Arizona Press (Tucson), 701
- Chauvin, G., et al. 2005, *A&A*, 438, L29
- Cochran, W. D., Endl, M., Wittenmyer, R. A., & Bean, J. L. 2007, *ApJ*, 665, 1407
- Cumming A., Marcy G. M., Butler R. P., 1999, *ApJ*, 526, 890
- Cumming, A. 2004, *MNRAS*, 354, 1165
- Cumming, A., Butler, R.P., Marcy, G.W., Vogt, S.S., Wright, J.T., & Fischer, D.A. 2008, *PASP*, 120, 531
- Demarque, P., Woo, J.-H., Kim, Y.-C., & Yi, S. K. 2004, *ApJS*, 155, 667
- Durisen, R. H., Boss, A. P., Mayer, L., Nelson, A. F., Quinn, T., & Rice, W. K. M. 2007, in *Protostars and Planets V*, B. Reipurth, D. Jewitt, and K. Keil (eds.), University of Arizona Press (Tucson), 607
- Eisner, J. A., & Kulkarni, S. R. 2001, *ApJ*, 561, 1107

- Endl, M., Kürster, M., Els, S., Hatzes, A. P., Cochran, W. D., Dennerl, K., Döbereiner, S. 2002, *A&A*, 392, 671
- Endl, M., Cochran, W. D., Kürster, M., Paulson, D. B., Wittenmyer, R. A., MacQueen, P. J., & Tull, R. G. 2006, *ApJ*, 649, 436
- Fischer, D. A., & Valenti, J. 2005, *ApJ*, 622, 1102
- Fischer, D. A., et al. 2005, *ApJ*, 620, 481
- Fischer, D. A., et al. 2007, *ApJ*, 675, 790
- Forveille, T., et al. 2008, *A&A*, 493, 645
- Frink, S., Mitchell, D. S., Quirrenbach, A., Fischer, D. A., Marcy, G. W., & Butler, R. P. 2002, *ApJ*, 576, 478
- Galland, F., Lagrange, A.-M., Udry, S., Chelli, A., Pepe, F., Beuzit, J.-L., & Mayor, M. 2005, *A&A*, 444, L21
- Gaudi, B. S., et al. 2008, *Science*, 319, 927
- Ge, J., et al. 2007, in *First Light Science with the GTC*, eds. R. Guzmán, C. Packham, J. M. Rodríguez-Espinosa, & S. Torres-Peimbert, *Revista Mexicana de Astronomía y Astrofísica (Serie de Conferencias)*, 29, 30
- Gonzalez G., 1997, *MNRAS*, 285, 403
- Hatzes, A. P., Guenther, E. W., Endl, M., Cochran, W. D., Dilling, M. P., & Bedalov, A. 2005, *A&A*, 437, 743
- Hekker, S., Snellen, I. A. G., Aerts, C., Quirrenbach, A., Reffert, S., & Mitchell, D. S. 2008, *A&A*, 480, 215
- Holmberg, J., Nordström, B., & Andersen, J. 2007, *A&A*, 475, 519
- Huélamo, N., et al. 2008, *A&A*, 489, L9
- Ida, S., & Lin, D. N. C. 2004, *ApJ*, 616, 567
- Ida, S., & Lin, D. N. C. 2005, *ApJ*, 626, 1045
- Johnson, J. A., Marcy, G. W., Fischer, D. A., Henry, G. W., Wright, J. T., Isaacson, H., & McCarthy, C. 2006, *ApJ*, 652, 1724

- Kalas, P., et al. 2008, *Science*, 322, 1345
- Kornet, K., Bodenheimer, P., Różyczka, M., & Stepinski, T. F. 2005, *A&A*, 430, 1133
- Kornet, K., Bodenheimer, P., & Różyczka, M. 2006, *A&A*, 458, 661
- Korzennik, S. G., Brown, T. M., Fischer, D. A., Nisenson, P., & Noyes, R. W. 2000, *ApJ*, 533, L147
- Latham, D. W. 1992, in *IAU Colloquium 135: Complementary Approaches to Double and Multiple Star Research*, H.A. McAlister & W.I. Hartkopf eds, *ASP Conf. Ser.*, 32, 110.
- Laughlin, G., Bodenheimer, P., & Adams, F. C. 2004, *ApJ*, 612, L73
- Lee, J. W., Kim, S.-L., Kim, C.-H., Koch, R. H., Lee, C.-U., Kim, H.-I., & Park, J.-H. 2009, *AJ*, 137, 3181
- Livio, M., & Pringle, J. E. 2003, *MNRAS*, 346, L42
- Lovis, C., et al. 2006, *Nature*, 441, 305
- Lovis, C., & Mayor, M. 2007, *A&A*, 472, 657
- Marois, C., Macintosh, B., Barman, T., Zuckerman, B., Song, I., Patience, J., Lafreniere, D., & Doyon, R. 2008, *Science*, 322, 1348
- Marcy, G., Butler, R. P., Fischer, D., Vogt, S. S., Wright, J. T., Tinney, C. G., & Jones, H. R. A. 2005, *Progress of Theoretical Physics*, 158, 24
- Matsuo, T., Shibai, H., Ootsubo, T., & Tamura, M. 2007, *ApJ*, 662, 1282
- Mayer L., Quinn T., Wadsley J., & Stadel J., 2004, *ApJ*, 609, 1045
- Mayer L., Lufkin, G., Quinn T., & Wadsley J., 2007, *ApJ*, 661, L77
- Mayor, M., & Queloz, D. 1995, *Nature*, 378, 355
- Mayor, M., et al. 2008, *A&A*, 493, 639
- McCarthy, C., & Zuckerman, B. 2004, *AJ*, 127, 2871
- Narayan, R., Cumming, A., Lin, D. N. C., 2005, *ApJ*, 620, 1002
- Nelson A. F., Angel J. R. P. 1998, *ApJ*, 500, 940

- Neuhäuser, R., Guenther, E. W., Wuchterl, G., Mugrauer, M., Bedalov, A., & Hauschildt, P. H. 2005, *A&A*, 435, L13
- Niedzielski, A., et al. 2007, *ApJ*, 669, 1354
- Paulson, D. B., Cochran, W. D., & Hatzes, A. P. 2004, *AJ*, 127, 3579
- Pasquini, L., et al., 2007, *A&A*, 473, 979
- Pollack, J. B., Hubickyj, O., Bodenheimer, P., Lissauer, J. J., Podolack, M., & Greenzweig, Y. 1996, *Icarus*, 124, 62
- Queloz, D., et al. 2001, *A&A*, 379, 279
- Rafikov, R. R. 2005, *ApJ*, 621, L69
- Reddy, B. E., Lambert, D. L., & Allende Prieto, C. 2006, *MNRAS*, 367, 1329
- Rice, W. K. M., Armitage, P. J., Bonnell, I. A., Bate, M. R., Jeffers, S. V., & Vine, S. G. 2003, *MNRAS*, 346, L36
- Rivera, E., Lissauer, J. J., Butler, R. P., Marcy, G. W., Vogt, S. S., Fischer, D. A., Brown, T., Laughlin, G., & Henry, G. W. 2005, *ApJ*, 634, 625
- Ryan, S. G., 1989 *AJ*, 98, 1693
- Ryan, S. G., & Norris, J. E. 1991, *AJ*, 101, 1835
- Saar, S. H., Butler, R. P., & Marcy, G. W. 1998, *ApJ*, 498, L153
- Santos, N. C., Mayor, M., Naef, D., Pepe, F., Queloz, D., Udry, S., & Blecha, A. 2000, *A&A*, 361, 265
- Santos, N. C., Israelian, G., & Mayor, M. 2004, *A&A*, 415, 1153
- Santos, N. C., Mayor, M., Bouchy, F., Pepe, F., Queloz, D., & Udry, S. 2007, *A&A*, 474, 647
- Sato, B., et al. 2003, *ApJ*, 597, L157
- Setiawan, J., Rodmann, J., da Silva, L., Hatzes, A. P., Pasquini, L., von der Lühe, O., de Medeiros, J. R., Döllinger, M. P., & Girardi, L. 2005, *A&A*, 437, L31
- Setiawan, J., Henning, Th., Launhardt, R., Müller, A., Weise, P., & Kürster, M. 2008, *Nature*, 451, 38

- Silvotti, R., et al. 2007, *Nature*, 449, 189
- Sousa, S. G., et al. 2008, *A&A*, 487, 373
- Sozzetti, A. 2005, *PASP*, 117, 1021
- Sozzetti, A., Torres, G., Latham, D. W., Carney, B. W., Stefanik, R. P., Boss, A. P., Laird, J. B., & Korzennik, S. G. 2006, *ApJ*, 649, 428 (S06)
- Sozzetti, A., et al. 2009, *ApJ*, 691, 1145
- Takeda, G., Ford, E. B., Sills, A., Rasio, F. A., Fischer, D. A., & Valenti, J. A. 2007, *ApJS*, 168, 297
- Udry, S., & Santos, N. C. 2007, *ARA&A*, 45, 397
- Udry, S., et al., 2007, *A&A*, 469, L43
- Unwin, S. C., et al. 2008, *PASP*, 120, 38
- Valenti, J. A., Butler, R. P., & Marcy, G. W. 1995, *PASP*, 107, 966
- Valenti, J. A., & Fischer, D. A. 2005, *ApJS*, 159, 41
- Venn, K. A., Irwin, M., Shetrone, M. D., Tout, C. A., Hill, V., & Tolstoy, E. 2004, *AJ*, 128, 1177
- Vogt, S. S., et al., 1994, in *Instrumentation in Astronomy VIII*, D. L. Crawford & E. R. Craine eds., *Proc. SPIE*, 2198, 362
- Wolf, V. M., & Wallerstein, G. 2005, *MNRAS*, 356, 963
- Zapatero Osorio, M. R., & Martín, E. L. 2004, *A&A*, 419, 167
- Walker, G. A. H., Walker, A. R., Irwin, A. W., Larson, A. M., Yang, S. L. S., Richardson, D. C. 1995, *Icarus*, 116, 359

Table 1. Target list of the Keck HIRES metal-poor planet survey

Star Name	Alt. Name (HD/HIP)	RA (J2000)	DEC (J2000)	V (mag)	T_{eff} (K)	[Fe/H] (dex)	M_{\star} (M_{\odot})	$B - V$	$V - K$	$\log g$ (dex)	d (phot) (pc)	d (Hip) (pc)
G 30-56 ...	HIP 1301 .	0 16 20.87	+16 38 46.9	9.73	5753	-0.66	0.89	0.57	1.49	4.47	103	115
G 158-102 .		0 35 41.26	-06 42 36.6	10.82	5320	-0.73	0.78	0.70	1.75	4.60	113	...
HD 3567 ...		0 38 31.95	-08 18 33.4	9.25	6010	-1.34	0.83	0.46	1.35	4.36	98	104
G 270-49 ...	HIP 3441 .	0 43 57.09	-07 32 01.0	9.38	5658	-0.66	0.85	0.58	1.56	4.53	84	91
G 70-17 ...		0 50 6.50	-04 25 55.8	11.29	4828	-0.82	0.64	0.88	2.30	4.71	84	...
G 2-19 ...	HD 6500 ..	1 6 5.15	+01 42 23.1	9.46	5618	-0.60	0.86	0.60	1.57	4.53	83	79
HD 7424 ...		1 14 7.24	-16 25 35.0	10.08	5538	-0.76	0.82	0.67	1.64	4.56	97	116
G 271-34 ..	HD 7983 ..	1 19 0.00	-08 56 22.2	8.90	5638	-0.73	0.85	0.59	1.53	4.52	65	67
HD 10519 .		1 42 14.85	-17 53 19.8	7.49	5561	-0.72	0.81	0.61	1.67	4.57	31	49
G 133-35 ...	HIP 8130 .	1 44 29.83	+44 27 50.0	10.18	5402	-0.61	0.81	0.68	1.75	4.58	95	88
G 159-5 ...	HIP 8720 .	1 52 10.47	-02 48 18.2	10.88	5092	-0.66	0.73	0.76	1.97	4.65	92	...
G 272-125 .	HIP 9056 .	1 56 37.95	-14 10 31.1	9.68	5393	-1.08	0.73	0.65	1.71	4.63	69	73
G 72-60 ...	HIP 9982 .	2 8 33.46	+31 23 25.6	10.28	5813	-0.84	0.86	0.56	1.53	4.47	138	260
G 74-5 ...	HIP 10140	2 10 24.53	+29 48 23.7	8.76	5630	-0.94	0.80	0.57	1.54	4.55	59	57
BD-01-306 .	HIP 10449	2 14 40.30	-01 12 05.1	9.08	5621	-0.96	0.81	0.57	1.52	4.54	70	62
G 94-49 ...		2 16 56.55	+27 24 48.4	10.40	5346	-0.88	0.74	0.66	1.77	4.63	94	...
G 4-10 ...	HD 14056 .	2 17 7.14	+21 34 0.5	9.05	5577	-0.72	0.83	0.62	1.58	4.55	65	69
G 94-70 ...	HD 15927 .	2 28 13.29	+25 50 48.5	9.37	5803	-0.70	0.89	0.53	1.46	4.47	92	...
G 36-28 ...	HD 16397 .	2 38 27.86	+30 48 59.9	7.36	5673	-0.58	0.90	0.58	1.50	4.49	34	36
G 76-30 ...	HIP 13037	2 47 32.19	+06 41 39.9	10.18	5073	-0.81	0.70	0.76	2.00	4.67	65	65
G 78-12 ...		3 2 7.31	+42 44 18.2	10.07	5204	-1.12	0.69	0.74	1.82	4.67	64	...
HD 19445 .		3 8 25.60	+26 19 53.2	8.06	5890	-2.12	0.75	0.45	1.37	4.48	45	39
G 77-35 ...	HIP 15126	3 15 4.76	+01 2 15.2	10.22	5393	-0.77	0.78	0.68	1.77	4.60	90	79
G 77-37 ...	HD 20369 .	3 16 45.68	+05 1 10.1	9.22	5598	-0.92	0.80	0.62	1.57	4.55	70	92
G 78-41 ...	HD 275573	3 34 57.15	+38 18 24.1	10.21	5437	-0.62	0.82	0.67	1.68	4.57	99	...
G 80-15 ...	HD 22879 .	3 40 22.07	-03 13 1.1	6.69	5827	-0.69	0.90	0.54	1.47	4.45	27	24
HD 23439A		3 47 2.11	+41 25 38.1	8.19	5026	-1.02	0.65	0.75	2.07	4.71	24	24
HD 25329 .		4 3 15.00	+35 16 23.9	8.51	4762	-1.73	0.54	0.87	2.29	4.80	17	18
G 81-8 ...	HD 276122	4 12 28.65	+41 59 26.0	10.53	5407	-1.01	0.74	0.64	1.71	4.63	106	...
G 8-16 ...	HD 284248	4 14 35.52	+22 21 4.2	9.24	6022	-1.67	0.79	0.42	1.33	4.41	96	78
G 82-5 ...	HIP 19814	4 14 57.75	-05 37 50.5	10.60	5325	-0.70	0.77	0.69	1.82	4.61	104	41
G 85-17 ...		4 49 52.76	+22 29 35.6	10.46	5482	-0.67	0.82	0.66	1.64	4.56	114	...
BD-22-1833		4 49 15.10	-22 38 7.1	11.20	4714	-1.26	0.57	0.86	2.36	4.76	68	...
G 83-50 ...	HD 32237 .	5 2 09.84	+14 04 54.2	8.24	5203	-0.61	0.76	0.72	1.92	4.63	33	29
G 84-37 ...	HD 241253	5 9 56.96	+05 33 26.7	9.72	5824	-1.01	0.84	0.52	1.43	4.46	111	97
G 248-45 ...	HIP 26452	5 37 39.57	+68 44 6.7	9.57	5854	-0.77	0.90	0.55	1.45	4.42	106	76
G 102-27 ...	HD 247297	5 45 40.38	+14 41 20.1	9.05	5494	-0.85	1.04	0.65	1.77	3.74	110	293
G 100-43 ...	HD 248175	5 50 31.01	+23 27 42.9	8.83	5274	-0.85	0.73	0.69	1.83	4.64	45	...
G 192-18 ...		6 6 38.02	+56 26 56.2	10.90	4735	-0.67	0.65	0.88	2.37	4.71	71	...
G 101-34 ...	HIP 30098	6 20 3.84	+38 20 44.1	10.76	4997	-1.31	0.94	0.74	2.10	2.64	...	1471
G 249-49 ...	HD 45205 .	6 30 15.67	+60 47 2.8	8.43	5820	-0.83	0.89	0.55	1.43	4.43	63	72
HD 46341 .		6 32 37.99	-06 29 18.5	8.62	5760	-0.71	0.89	0.56	1.46	4.47	67	59
G 103-53 ...		6 43 46.47	+25 31 30.3	10.19	5344	-0.80	0.76	0.68	1.75	4.61	86	...
G 107-43 ...		7 2 7.16	+36 56 58.8	10.27	5603	-0.78	1.06	0.64	1.68	3.79	187	...
G 110-38 ...		7 6 54.13	+18 8 11.1	11.34	4924	-0.63	0.69	0.79	2.23	4.69	107	...
G 87-27 ...	HIP 34613	7 10 8.30	+37 16 33.9	9.84	5140	-0.68	1.10	0.81	2.09	3.49	244	200
G 193-33 ...	HD 233345	7 10 29.79	+53 15 6.4	8.88	5647	-0.63	1.11	0.58	1.60	3.80	98	93
G 88-20 ...	HD 56513 .	7 18 28.87	+27 15 10.3	8.05	5521	-0.64	0.83	0.62	1.64	4.56	42	35
G 88-31 ...	HD 59374 .	7 30 29.02	+18 57 40.6	8.49	5781	-0.83	0.83	0.52	1.51	4.52	61	50
G 88-40 ...	HD 60319 .	7 34 35.11	+16 54 4.0	8.94	5862	-0.86	0.87	0.50	1.43	4.46	81	82
HD 64090 .		7 53 33.12	+30 36 18.3	8.28	5384	-1.75	0.65	0.61	1.75	4.70	30	28
G 193-80 ...	HD 64412 .	7 56 44.20	+56 12 20.3	8.78	5625	-0.79	0.81	0.58	1.57	4.55	60	59
G 9-47 ...	HD 78050 .	9 6 42.93	+20 30 35.5	7.68	5014	-1.08	1.00	0.80	2.12	2.91	166	376
G 116-15 ...		9 15 55.00	+40 14 35.6	10.39	5494	-0.66	0.82	0.64	1.63	4.56	120	...
G 235-45 ...	HIP 48209	9 49 42.82	+65 18 15.0	9.67	5387	-0.71	0.80	0.70	1.68	4.58	75	86
G 42-34 ...		10 3 12.28	+19 50 26.9	10.70	4719	-1.01	0.61	0.85	2.33	4.74	60	...
G 44-6 ...	HD 88725	10 14 8.33	+03 9 4.7	7.75	5629	-0.61	0.87	0.61	1.54	4.52	39	36
HD 94028 .		10 51 28.13	+20 16 39.0	8.22	5936	-1.56	0.79	0.47	1.37	4.43	55	52
G 122-23 ...	HD 233832	11 26 5.48	+50 22 32.8	10.09	4941	-0.74	0.69	0.83	2.08	4.68	56	64
HD 103095		11 52 58.77	+37 43 7.2	6.43	5014	-1.44	0.60	0.75	2.02	4.75	10	9
G 122-57 ...	HD 103912	11 58 0.08	+48 12 12.4	8.36	4949	-0.66	1.12	0.86	2.17	2.94	219	180
G 11-36 ...	HD 104800	12 4 5.56	+03 20 26.7	9.25	5623	-0.76	0.82	0.58	1.58	4.55	73	63
G 59-1 ...	HIP 59233	12 08 54.66	+21 47 19.4	9.52	5335	-1.05	0.70	0.63	1.82	4.66	61	113
G 197-45 ...		12 9 28.90	+51 56 1.0	10.73	5144	-0.92	0.69	0.72	1.92	4.68	88	...
G 237-48 ...	HD 105791	12 10 25.44	+65 39 43.8	8.68	5542	-1.68	0.88	0.56	1.65	3.61	122	216
G 197-51 ...		12 14 10.20	+53 35 28.3	9.63	5751	-0.64	0.89	0.56	1.48	4.48	106	...

Table 1—Continued

Star Name	Alt. Name (HD/HIP)	RA (J2000)	DEC (J2000)	V (mag)	T_{eff} (K)	[Fe/H] (dex)	M_{\star} (M_{\odot})	$B - V$	$V - K$	$\log g$ (dex)	d (phot) (pc)	d (Hip) (pc)
G 59-18		12 23 31.02	+16 54 9.2	10.18	5159	-1.35	0.93	0.72	1.97	3.14	408	...
G 123-29	HD 108076	12 24 45.89	+38 19 7.5	8.05	5705	-0.76	0.85	0.57	1.57	4.52	47	37
G 13-38	HIP 60747.	12 26 59.86	+01 33 58.3	10.48	5241	-0.87	0.73	0.70	1.83	4.65	89	91
G 60-26	HIP 61802.	12 39 59.37	+12 38 32.1	9.82	5435	-1.35	0.92	0.65	1.85	3.64	189	220
G 14-5	HD 111515	12 49 44.83	+01 11 16.9	8.14	5366	-0.70	0.78	0.68	1.76	4.60	35	33
G 164-34	HIP 63336.	12 58 42.95	+33 14 44.6	10.24	5453	-0.72	0.80	0.64	1.67	4.58	105	84
G 237-84	HD 112956	12 58 49.26	+68 47 6.9	8.07	5347	-0.66	0.79	0.68	1.75	4.59	34	34
G 62-9		13 3 18.24	+04 7 27.5	11.31	5017	-0.63	0.72	0.78	2.05	4.66	109	...
G 63-5	HD 114606	13 11 21.40	+09 37 33.5	8.74	5516	-0.62	0.83	0.62	1.66	4.56	55	61
G 61-38	HIP 64386.	13 11 48.31	+18 22 44.8	9.89	5510	-0.75	0.81	0.64	1.67	4.57	89	70
BD-22-3557		13 19 11.64	-23 1 13.5	10.26	4939	-0.74	0.67	0.83	2.16	4.70	60	...
G 63-44	HD 118659	13 38 00.4	+19 08 53.0	8.83	5456	-0.61	0.82	0.68	1.71	4.57	51	53
G 63-46	HIP 66665.	13 39 59.57	+12 35 21.7	9.39	5691	-0.84	0.82	0.58	1.55	4.53	84	134
G 135-46	HIP 70324.	14 23 20.04	+18 33 35.5	9.36	5515	-0.62	0.84	0.62	1.64	4.55	75	77
HD 126681 . . .		14 27 24.91	-18 24 40.4	9.31	5475	-1.38	0.69	0.60	1.66	4.65	61	52
G 66-22	HIP 71979.	14 43 17.97	+05 49 39.8	10.46	5166	-1.14	0.65	0.70	2.03	4.71	77	88
G 223-82		14 47 56.57	+62 56 6.2	11.26	4795	-0.86	0.64	0.85	2.24	4.72	85	...
G 178-50		14 48 12.32	+41 31 13.7	10.56	5106	-0.68	0.74	0.75	1.96	4.65	85	...
G 151-10	HD 131653	14 55 7.07	-09 5 50.3	9.52	5287	-0.70	0.76	0.72	1.85	4.62	61	49
G 66-51		15 0 50.07	+02 7 37.5	10.63	5194	-1.08	0.69	0.71	1.88	4.68	86	...
G 179-11	HD 133564	15 1 36.76	+44 59 25.3	8.84	5600	-0.57	0.88	0.62	1.57	4.52	63	55
G 66-55	HIP 73626.	15 3 0.65	+08 41 3.7	11.39	4968	-0.65	0.70	0.80	2.09	4.68	110	147
G 15-7	HIP 74123.	15 8 53.84	-03 47 0.7	10.49	5280	-0.88	0.74	0.72	1.79	4.64	91	81
G 167-21		15 8 49.15	+28 39 08.8	11.59	4867	-0.75	0.67	0.84	2.19	4.70	106	...
HD 134440 . . .		15 10 12.97	-16 27 46.5	9.46	4751	-1.52	0.55	0.85	2.29	4.78	29	29
HD 134439 . . .		15 10 13.09	-16 22 45.8	9.09	4946	-1.57	0.58	0.76	2.06	4.77	31	29
LHS 3038	HIP 74477.	15 13 5.78	-21 58 39.4	11.27	4739	-0.80	0.63	0.90	2.37	4.72	77	64
G 179-22	HIP 74588.	15 14 26.18	+33 0 38.2	10.69	5114	-1.32	0.93	0.71	1.98	3.05	522	332
G 16-13	HIP 77637.	15 50 58.94	+08 25 23.7	10.00	5595	-1.09	0.98	0.59	1.66	3.74	183	276
G 153-21	HIP 78620.	16 3 0.17	-06 27 11.2	10.19	5714	-0.64	0.89	0.71	1.84	4.48	107	92
G 16-31	HIP 79117.	16 8 55.40	+01 51 7.3	10.16	4844	-0.67	0.68	0.85	2.20	4.69	55	50
G 17-10		16 19 43.56	+03 1 1.0	11.25	4781	-0.67	0.67	0.90	2.27	4.70	83	...
G 17-16	HD 148408	16 27 48.22	-01 4 8.8	9.63	5273	-0.87	0.73	0.72	1.82	4.64	62	...
HD 148211 . . .		16 27 12.90	-22 7 36.5	7.70	5733	-0.83	1.04	0.55	1.50	3.82	59	53
HD 148816 . . .		16 30 28.46	+04 10 41.6	7.29	5826	-0.72	0.89	0.54	1.45	4.46	37	41
G 169-45	HIP 83604.	17 5 19.32	+26 56 10.9	10.03	5664	-0.66	0.86	0.60	1.57	4.52	112	159
HD 157089 . . .		17 21 7.05	+01 26 35.0	6.96	5730	-0.60	0.89	0.58	1.51	4.49	29	39
G 19-27	HD 158809	17 31 25.40	-02 32 19.7	8.15	5515	-0.63	1.11	0.65	1.70	3.78	70	75
G 139-49		17 36 48.11	+02 50 19.6	10.70	5340	-1.20	0.70	0.67	1.79	4.66	100	...
BD+18-3423	HIP 86321.	17 38 15.61	+18 33 25.5	9.77	5943	-1.00	0.86	0.49	1.39	4.43	124	112
G 240-68	HIP 86830.	17 44 32.87	+67 17 42.4	9.70	5347	-0.66	1.10	0.70	1.82	3.74	148	140
G 204-30		17 49 58.63	+37 31 18.6	10.27	5581	-0.97	0.77	0.60	1.59	4.58	112	...
G 140-33	HIP 88365.	18 2 38.97	+04 28 50.1	10.69	5261	-1.06	0.71	0.71	1.85	4.66	97	110
G 204-49		18 12 21.88	+05 24 4.4	10.85	5121	-1.04	0.68	0.73	1.95	4.69	88	...
G 140-46	HIP 89215.	18 12 35.80	+40 33 24.1	10.43	5034	-1.26	0.62	0.73	2.08	4.74	67	59
HD 171620 . . .		18 34 30.7	+34 24 56.0	7.56	6045	-0.41	1.05	0.50	1.30	4.29	51	52
G 22-6	HD 175179	18 54 23.20	-04 36 18.6	9.08	5594	-0.78	0.80	0.58	1.63	4.57	69	84
G 184-42	HD 230409	19 0 43.33	+19 4 28.4	10.08	5318	-1.03	0.73	0.70	1.76	4.64	78	64
HD 177095 . . .		19 3 56.71	-20 27 36.6	9.64	5443	-0.76	0.78	0.62	1.78	4.60	75	61
HD 177758 . . .		19 6 25.32	-11 53 50.7	7.23	5667	-0.76	1.06	0.57	1.55	3.80	48	39
G 22-20	HD 179626	19 13 20.72	-00 35 42.3	9.22	5780	-1.17	0.78	0.52	1.59	4.54	81	133
G 142-21	HD 180164	19 15 8.15	+10 34 31.5	9.41	5880	-1.04	0.86	0.52	1.44	4.42	96	...
BD+41-3306	HIP 94931.	19 19 0.55	+41 38 4.6	8.86	4905	-0.87	0.65	0.83	2.12	4.71	31	35
HD 184499 . . .		19 33 27.08	+33 12 6.7	6.62	5659	-0.66	1.09	0.58	1.50	3.83	35	32
G 208-32		19 37 54.53	+44 59 4.6	9.64	5819	-1.03	0.84	0.51	1.47	4.47	105	...
G 92-19		19 39 14.72	-02 36 44.7	10.31	5400	-0.87	0.76	0.66	1.75	4.62	97	...
HD 188510 . . .		19 55 9.68	+10 44 27.4	8.83	5497	-1.75	0.68	0.59	1.68	4.66	44	39
HD 189558 . . .		20 1 0.25	-12 15 20.3	7.74	5639	-1.24	0.94	0.57	1.58	3.75	69	68
BD+23-3912	HD 345957	20 10 48.16	+23 57 54.5	8.88	5852	-1.37	0.79	0.51	1.47	4.46	67	107
BD-15-5584	HD 192031	20 13 22.58	-15 25 55.6	8.66	5223	-0.94	0.71	0.71	1.85	4.66	36	37
G 186-18		20 16 38.65	+29 31 50.6	11.39	4991	-0.59	0.71	0.82	2.20	4.67	105	...
HD 192718 . . .		20 16 38.08	-07 26 37.9	8.40	5717	-0.63	0.88	0.57	1.51	4.50	56	58
G 143-43	HD 351944	20 17 1.34	+17 15 45.9	10.75	5121	-0.78	0.71	0.75	1.95	4.66	91	...
G 24-13	HIP 100279	20 20 24.56	+06 01 52.8	10.13	5688	-0.71	0.86	0.62	1.63	4.51	113	98
HD 193901 . . .		20 23 35.85	-21 22 14.2	8.66	5711	-1.24	0.76	0.56	1.52	4.56	54	44
HD 194598 . . .		20 26 11.92	+09 27 0.4	8.35	5890	-1.28	0.82	0.49	1.38	4.42	60	56

Table 1—Continued

Star Name	Alt. Name (HD/HIP)	RA (J2000)	DEC (J2000)	V (mag)	T_{eff} (K)	[Fe/H] (dex)	M_* (M_{\odot})	$B - V$	$V - K$	$\log g$ (dex)	d (phot) (pc)	d (Hip) (pc)
G 24-17	HIP 101146	20 30 08.49	+04 34 17.6	11.47	4768	-0.99	0.61	0.87	2.35	4.73	85	93
HD 195137 . . .		20 30 05.81	-16 14 13.1	9.89	5552	-1.02	0.75	0.64	1.77	4.60	85	...
G 144-9	HIP 101369	20 32 43.02	+19 31 35.4	11.66	4723	-0.89	0.62	0.87	2.37	4.73	94	99
LP 755-059 . .		20 32 39.97	-11 17 52.3	10.60	5052	-0.67	0.74	0.80	1.97	4.64	78	...
HD 196892 . . .		20 40 49.38	-18 47 33.3	8.23	5917	-1.00	0.87	0.50	1.41	4.41	57	63
BD+04-4551 . .	HIP 102718	20 48 50.72	+05 11 58.8	9.61	5783	-1.55	0.74	0.51	1.49	4.54	88	610
G 25-5		20 49 20.62	+01 55 30.1	10.11	5479	-0.57	0.85	0.67	1.66	4.55	96	...
G 144-52	HIP 103812	21 2 12.17	+19 54 3.2	9.07	5500	-0.62	0.84	0.65	1.62	4.55	62	58
G 187-18	HD 335471	21 3 6.13	+29 28 56.2	10.19	5555	-0.88	0.79	0.61	1.60	4.58	106	127
HD 201889 . . .		21 11 59.52	+24 10 5.3	8.06	5570	-0.90	1.02	0.59	1.61	3.76	73	56
HD 201891 . . .		21 11 59.03	+17 43 39.9	7.37	5851	-1.42	0.79	0.51	1.42	4.44	35	35
G 25-29	HD 204155	21 26 42.91	+05 26 29.9	8.50	5702	-0.70	0.86	0.57	1.51	4.51	56	77
G 126-36		21 48 19.29	+19 58 30.6	9.95	5536	-1.05	0.76	0.61	1.60	4.59	93	...
LP 819-002 . . .		21 57 04.19	-18 00 35.0	11.46	5047	-0.86	0.69	0.78	2.03	4.68	113	...
HD 210295 . . .		22 09 41.45	-13 36 19.5	9.57	4754	-1.49	0.90	0.89	2.38	2.80	949	394
G 241-7		22 25 42.74	+69 31 35.7	10.50	5546	-0.87	0.80	0.62	1.60	4.56	119	...
G 241-18	HD 215065	22 40 54.6	+66 31 24.0	7.46	5544	-0.56	0.86	0.63	1.61	4.54	31	29
G 27-44	HD 215257	22 43 50.72	+03 53 12.6	7.42	5828	-0.78	0.85	0.50	1.53	4.51	39	42
G 28-15		22 45 43.33	-01 43 32.2	11.26	5195	-0.49	0.81	0.79	1.92	4.60	125	...
G 28-16		22 47 38.51	+06 25 19.9	11.59	4907	-1.03	0.63	0.81	2.22	4.73	99	...
G 28-17	HD 216179	22 50 45.94	+01 51 54.6	9.34	5375	-0.74	0.77	0.68	1.78	4.61	61	60
G 241-42	HD 218209	23 5 6.09	+68 25 1.4	7.48	5473	-0.64	0.82	0.65	1.68	4.57	28	30
G 28-43		23 9 34.00	+00 43 30.0	9.94	5070	-1.76	0.59	0.70	1.99	4.77	48	...
G 28-48		23 13 0.52	+01 48 11.6	11.11	4982	-0.56	0.73	0.87	2.11	4.66	94	...
G 29-20	HD 219715	23 18 1.20	+09 4 28.1	9.17	5158	-1.07	0.99	0.75	1.99	3.38	190	...
G 68-10	HD 220197	23 21 58.29	+16 37 57.1	8.96	5564	-0.65	0.83	0.61	1.61	4.55	65	67
G 68-30	HD 221876	23 35 42.5	+20 34 49.0	9.08	5809	-0.60	0.94	0.56	1.45	4.43	81	75
G 157-93	HD 222766	23 43 34.92	-07 55 24.0	10.12	5409	-0.78	0.78	0.66	1.74	4.60	89	118

Note. — Target list of the Keck/HIRES metal-poor planet search program. We provide visual magnitude, effective temperature, metallicity, mass, colors, surface gravity, and distance estimates

Table 2. Radial-velocity results for all stars

Star Name	N	σ_{rms} (m s ⁻¹)	$\bar{\sigma}_{\text{int}}$ (m s ⁻¹)	ΔT (days)
G30-56....	5	21.4	6.9	378.0
G158-102..	5	7.2	10.2	378.0
HD3567...	3	11.1	8.8	115.7
G270-49...	5	10.5	9.8	378.0
G70-17....	5	7.7	11.7	378.0
G2-19.....	5	12.9	11.7	377.9
HD7424...	6	236.0	6.7	492.7
G271-34...	5	13.6	11.1	377.0
HD10519..	3	4.6	7.1	115.7
G133-35...	3	17.2	5.9	115.8
G159-5....	6	14.3	16.5	650.2
G272-125..	3	8.9	6.0	115.7
G72-60....	2	11.0	11.0	872.7
G74-5.....	5	12.0	8.7	650.1
BD-01-306	5	15.5	9.0	650.2
G94-49....	4	10.3	5.6	650.1
G4-10.....	5	11.8	7.9	650.2
G94-70....	5	9.9	9.2	764.9
G36-28....	7	19.6	9.3	2819.1
G76-30....	5	10.2	8.7	764.8
G78-12....	2	8.4	7.2	1.0
HD19445..	6	19.6	17.8	2675.7
G77-35....	4	7.6	9.9	764.8
G77-37....	5	16.9	9.0	764.8
G78-41....	3	19.4	5.7	764.9
G80-15....	5	11.3	9.7	764.8
HD23439A	5	5.9	5.1	764.9
HD25329..	4	16.4	5.7	764.9
G81-8.....	2	2.9	6.7	764.9
G8-16.....	3	5.8	10.1	764.9

Table 2—Continued

Star Name	N	σ_{rms} (m s ⁻¹)	$\bar{\sigma}_{\text{int}}$ (m s ⁻¹)	ΔT (days)
G82-5	3	19.4	8.7	764.9
G85-17	3	4.7	6.3	764.8
BD-22-1833	2	3.5	9.1	1.0
G83-50	5	11.2	13.0	2821.1
G84-37	2	8.2	8.9	764.9
G248-45	3	4.0	9.8	764.8
G102-27	3	8.3	7.8	764.9
G100-43	3	6.9	7.8	764.9
G192-18	3	9.0	10.2	764.9
G101-34	3	7.3	5.4	764.9
G249-49	5	8.2	8.3	2137.0
HD46341	3	5.0	6.7	764.0
G103-53	4	18.9	8.8	1006.0
G107-43	3	6.9	7.0	764.9
G110-38	4	8.1	18.2	1006.1
G193-33	5	9.7	9.6	1006.1
G87-27	5	11.8	9.2	1006.1
G88-20	7	14.8	10.3	1629.3
G88-31	6	20.9	16.5	2056.3
G88-40	4	9.2	12.9	1006.1
HD64090	8	9.9	13.3	1629.3
G193-80	5	8.2	9.2	1006.1
G9-47	7	11.5	6.5	1006.1
G116-15	5	7.4	8.2	1006.1
G235-45	5	7.0	10.2	1006.2
G42-34	5	6.9	8.0	1006.1
G44-6	5	9.6	8.0	2821.2
HD94028	8	14.1	13.2	2393.2
G122-23	5	18.1	11.5	889.7
HD103095	6	17.1	16.6	889.7

Table 2—Continued

Star Name	N	σ_{rms} (m s ⁻¹)	$\bar{\sigma}_{\text{int}}$ (m s ⁻¹)	ΔT (days)
G122-57...	6	8.8	7.9	889.7
G11-36....	4	13.1	9.9	407.9
G59-1.....	4	27.2	14.2	407.0
G197-45...	6	41.4	7.4	889.7
G237-48...	6	16.6	16.6	889.7
G197-51...	6	10.4	8.2	889.7
G59-18....	4	15.4	9.1	407.9
G123-29...	10	8.3	14.7	1916.8
G13-38....	5	10.7	11.0	407.9
G60-26....	4	20.3	10.3	407.9
G14-5.....	7	10.3	5.9	2705.7
G164-34...	5	5.5	10.5	889.7
G237-84...	9	54.7	11.5	2276.7
G62-9.....	4	10.6	13.5	407.9
G61-38....	4	9.5	10.2	407.9
G63-5.....	7	42.8	9.5	2704.7
BD-22-3557	6	10.7	11.6	891.6
G63-44....	7	16.2	8.5	2704.8
G63-46....	4	3.6	12.8	407.9
G135-46...	9	187.0	6.0	891.6
HD126681.	6	13.5	10.5	891.7
G66-22....	4	8.1	11.9	407.9
G223-82...	3	7.0	8.5	407.0
G178-50...	5	6.2	7.5	889.7
G151-10...	7	14.5	10.9	891.7
G66-51....	6	8.5	5.7	890.7
G179-11...	5	15.5	8.0	2276.7
G66-55....	6	5.5	11.6	890.7
G15-7.....	6	8.5	9.3	890.7
G167-21...	2	3.6	5.3	1.0

Table 2—Continued

Star Name	N	σ_{rms} (m s^{-1})	$\bar{\sigma}_{\text{int}}$ (m s^{-1})	ΔT (days)
HD134439..	6	9.5	9.1	891.6
HD134440..	6	9.6	9.5	891.6
LHS3038...	6	6.9	9.6	891.7
G179-22....	5	9.9	7.2	889.7
G16-13.....	5	12.7	9.2	757.0
G153-21....	5	7.6	9.8	757.0
G16-31.....	5	14.8	13.7	407.9
G17-10.....	7	5.2	11.4	889.8
G17-16.....	7	12.1	12.8	890.7
HD148211..	3	4.4	11.0	47.8
HD148816..	10	8.5	11.5	2494.1
G169-45....	5	16.6	12.5	396.7
HD157089..	13	9.5	10.5	2902.0
G19-27.....	18	16.9	6.9	891.8
G139-49....	4	8.5	8.6	757.0
BD+18-3423	2	7.7	4.8	1.9
G240-68....	5	7.7	12.1	756.8
G204-30....	4	12.8	11.0	394.9
G140-33....	4	5.4	11.5	757.0
G204-49....	5	8.0	7.9	756.8
G140-46....	5	11.8	12.0	757.0
HD171620..	6	6.5	6.7	2200.8
G22-6.....	5	7.6	8.0	757.0
G184-42....	5	5.0	8.6	757.8
HD177095..	5	6.9	11.1	757.0
HD177758..	5	4.9	11.2	377.9
G22-20.....	5	1.4	8.4	757.0
G142-21....	5	12.4	12.2	377.9
BD+41-3306	5	7.5	7.1	756.8
HD184499..	6	13.2	14.6	757.9

Table 2—Continued

Star Name	N	σ_{rms} (m s^{-1})	$\bar{\sigma}_{\text{int}}$ (m s^{-1})	ΔT (days)
G208-32	5	13.3	10.8	757.9
G92-19	5	4.9	10.5	757.0
HD188510	12	14.6	15.3	2901.0
HD189558	6	7.7	10.6	872.8
BD+23-3912	6	14.7	7.7	757.9
BD-15-5584	6	8.5	12.3	872.8
G186-18	5	3.3	11.6	377.9
HD192718	11	300.1	10.3	2285.8
G143-43	6	8.8	11.6	756.9
G24-13	5	8.1	14.2	475.8
HD193901	5	1.7	7.4	758.0
HD194598	5	14.5	10.9	756.0
G24-17	5	12.6	11.4	475.8
HD195137	6	20.6	7.1	475.0
G144-9	5	4.6	16.8	475.7
LP755-059	5	7.4	12.0	758.0
HD196892	5	7.0	12.5	758.0
BD+04-4551	4	10.3	12.5	758.0
G25-5	5	7.7	13.0	757.0
G144-52	5	7.1	10.3	757.0
G187-18	5	16.7	8.8	757.9
HD201889	3	6.8	7.2	380.0
HD201891	10	9.9	12.3	2901.0
G25-29	7	18.6	10.1	872.7
G126-36	4	13.1	9.3	407.9
LP819-002	5	6.1	14.4	475.7
HD210295	6	42.2	9.3	360.0
G241-7	4	2.6	12.3	872.6
G241-18	5	6.3	6.9	2285.8
G27-44	7	41.2	6.5	2900.1

Table 2—Continued

Star Name	N	σ_{rms} (m s ⁻¹)	$\bar{\sigma}_{\text{int}}$ (m s ⁻¹)	ΔT (days)
G28-15....	5	4.5	11.6	407.9
G28-16....	3	10.5	11.8	115.7
G28-17....	5	7.1	5.5	407.9
G241-42...	7	8.4	12.6	1793.1
G28-43....	6	408.1	30.0	522.7
G28-48....	5	8.3	10.1	407.9
G29-20....	5	10.3	7.0	407.9
G68-10....	5	9.4	6.7	407.9
G68-30....	7	6.7	6.7	2559.0
G157-93...	3	10.0	4.4	115.7

Note. — Radial-velocity results for all stars observed at least twice during the survey. For each star, we list the total number of spectra collected N , the total RV scatter σ_{rms} , the average internal measurement error $\bar{\sigma}_{\text{int}}$, and the time-span of the observations ΔT

Table 3. Variability analysis for the sample

Star Name	N	$\left(\frac{\sigma_{\text{rms}}}{\sigma_{\text{int}}}\right)_{\text{const}}$	$\text{Pr}(\chi^2_{\nu})$	$\text{Pr}(Ku)$	$\text{Pr}(F)$
G30-56	5	3.083	0.00000	0.03179	6.17e-05
G158-102..	5	0.713	0.69393	0.60753	0.97951
HD3567 . . .	3	1.251	0.070947	...	0.28643
G270-49 . . .	5	1.073	0.28123	0.28040	0.35165
G70-17	5	0.657	0.64313	0.91370	0.77199
G2-19	5	1.102	0.04342	0.33624	0.03304
HD7424 . . .	6	35.169	0.00000	0.00014	2.80e-45
G271-34 . . .	5	1.224	0.10093	0.07288	0.06761
HD10519..	3	0.651	0.50957	...	0.74858
G133-35 . . .	3	2.912	0.00000	...	0.00344
G159-5	6	0.864	0.51420	0.97616	0.01598
G272-125..	3	1.472	0.00121	...	0.35709
G72-60	2	1.007	0.13147	...	0.06534
G74-5	5	1.379	0.01229	0.18775	0.25586
BD-01-306	5	1.706	0.00047	0.46470	0.04737
G94-49	4	1.833	0.00139	0.30889	0.27614
G4-10	5	1.486	1.93e-06	0.86802	0.32619
G94-70	5	1.075	0.24947	0.67959	0.50209
G36-28	7	2.107	0.00000	0.00592	0.00297
G76-30	5	1.162	0.07179	0.60753	0.20927
G78-12	2	1.170	0.07897	...	0.39420
HD19445..	6	1.098	0.16878	0.17016	0.00083
G77-35	4	0.766	0.00636	0.92035	0.88406
G77-37	5	1.875	0.00154	0.28040	0.01256
G78-41	3	3.364	4.17e-07	...	0.01351
G80-15	5	1.158	0.10703	0.46470	0.24950
HD23439A	5	1.141	0.00660	0.60753	0.77597
HD25329..	4	2.875	0.00000	0.14581	0.01041
G81-8	2	0.429	0.54018	...	0.71816
G8-16	3	0.582	0.57097	...	0.84434
G82-5	3	2.225	0.00081	...	0.00126

Table 3—Continued

Star Name	N	$\left(\frac{\sigma_{\text{rms}}}{\sigma_{\text{int}}}\right)_{\text{const}}$	$\text{Pr}(\chi^2_\nu)$	$\text{Pr}(Ku)$	$\text{Pr}(F)$
G85-17	3	0.741	0.40111	...	0.70990
BD-22-1833	2	0.388	0.71530	...	0.86370
G83-50	5	0.864	0.28241	0.81241	0.18635
G84-37	2	0.922	0.18317	...	0.45097
G248-45 ...	3	0.414	0.80178	...	0.59685
G102-27 ...	3	1.055	0.20431	...	0.67486
G100-43 ...	3	0.888	0.33113	...	0.98285
G192-18 ...	3	0.891	0.15325	...	0.58525
G101-34 ...	3	1.367	0.04714	...	0.58108
G249-49 ...	5	0.991	0.12873	0.28040	0.79670
HD46341 ..	3	0.744	0.36459	...	0.89960
G103-53 ...	4	2.137	0.00023	0.03508	0.00439
G107-43 ...	3	0.985	0.33746	...	0.86211
G110-38 ...	4	0.443	0.83752	0.77589	0.66197
G193-33 ...	5	1.014	0.30018	0.74877	0.33614
G87-27	5	1.286	0.01788	0.53516	0.09887
G88-20	7	1.427	0.01917	0.07399	0.01956
G88-31	6	1.271	0.23852	0.58523	0.00053
G88-40	4	0.715	0.54877	0.99893	0.70679
HD64090 ..	8	0.746	0.64959	0.90738	0.21115
G193-80 ...	5	0.885	0.21504	0.91370	0.65457
G9-47	7	1.765	0.00049	0.03632	0.22684
G116-15 ...	5	0.896	0.31524	0.81241	0.84552
G235-45 ...	5	0.687	0.45070	0.97254	0.99424
G42-34	5	0.860	0.11729	0.97254	0.94333
G44-6	5	1.204	0.20855	0.33624	0.34969
HD94028 ..	8	1.065	0.31439	0.69762	0.09292
G122-23 ...	5	1.575	0.01311	0.04238	0.00184
HD103095 .	6	1.030	0.18916	0.02955	0.00337
G122-57 ...	6	1.117	0.11013	0.99669	0.95598
G11-36	4	1.320	0.08337	0.33525	0.06467

Table 3—Continued

Star Name	N	$\left(\frac{\sigma_{\text{rms}}}{\sigma_{\text{int}}}\right)_{\text{const}}$	$\text{Pr}(\chi^2_\nu)$	$\text{Pr}(Ku)$	$\text{Pr}(F)$
G59-1	4	1.918	0.00151	0.00603	0.00015
G197-45 . . .	6	5.594	0.00000	0.00309	8.66e-11
G237-48 . . .	6	0.999	0.32429	0.48294	0.00455
G197-51 . . .	6	1.267	0.02781	0.53358	0.39827
G59-18	4	1.684	0.01519	0.16160	0.01465
G123-29 . . .	10	0.566	0.95409	0.55365	0.74824
G13-38	5	0.978	0.30135	0.86802	0.26977
G60-26	4	1.966	0.00027	0.02676	0.00470
G14-5	7	1.737	0.00104	0.81451	0.70286
G164-34 . . .	5	0.530	0.87195	0.53516	0.44086
G237-84 . . .	9	4.747	0.00000	3.87e-06	4.58e-19
G62-9	4	0.789	0.50495	0.21669	0.23449
G61-38	4	0.938	0.24017	0.64925	0.57470
G63-5	7	4.497	0.00000	0.00115	2.39e-12
BD-22-3557	6	0.924	0.51613	0.84824	0.24135
G63-44	7	1.893	0.00027	0.09099	0.01075
G63-46	4	0.287	0.93275	0.58266	0.20744
G135-46 . . .	9	31.016	0.00000	2.01e-06	1.02e-39
HD126681 . .	6	1.286	0.02619	0.17016	0.06342
G66-22	4	0.686	0.59214	0.68211	0.90343
G223-82 . . .	3	0.822	0.43085	...	0.74902
G178-50 . . .	5	0.835	0.52415	0.86802	0.63270
G151-10 . . .	7	1.323	0.00060	0.55656	0.02458
G66-51	6	1.501	0.04533	0.84824	0.59215
G179-11 . . .	5	1.947	0.00183	0.74877	0.03493
G66-55	6	0.474	0.93100	0.91589	0.31431
G15-7	6	0.920	0.46356	0.73784	0.74457
G167-21 . . .	2	0.687	0.33124	...	0.82557
HD134439 . .	6	1.053	0.18208	0.82816	0.79079
HD134440 . .	6	1.008	0.21685	0.03641	0.37808
LHS3038 . . .	6	0.719	0.69710	0.07230	0.73659

Table 3—Continued

Star Name	N	$\left(\frac{\sigma_{\text{rms}}}{\sigma_{\text{int}}}\right)_{\text{const}}$	$\text{Pr}(\chi^2_\nu)$	$\text{Pr}(Ku)$	$\text{Pr}(F)$
G179-22	5	1.363	0.01181	0.81241	0.58010
G16-13	5	1.378	0.03664	0.28040	0.17171
G153-21	5	0.775	0.56228	0.74877	0.82049
G16-31	5	1.081	0.05528	0.00902	0.00750
G17-10	7	0.461	0.75762	0.25903	0.14925
G17-16	7	0.940	0.42784	0.09863	0.13011
HD148211 . . .	3	0.400	0.78876	...	0.74878
HD148816 . . .	10	0.739	0.82045	0.89063	0.85202
G169-45	5	1.321	0.07062	0.00902	0.00340
HD157089 . . .	13	0.906	0.54669	0.27370	0.54719
G19-27	18	2.456	0.00000	0.04334	0.00016
G139-49	4	0.990	0.15463	0.36286	0.56362
BD+18-3423 . .	2	1.607	0.01811	...	0.45879
G240-68	5	0.638	0.61794	0.91370	0.78553
G204-30	4	1.167	0.13306	0.28382	0.06969
G140-33	4	0.469	0.79242	0.80470	0.47432
G204-49	5	1.008	0.06007	0.74877	0.71747
G140-46	5	0.984	0.09430	0.81241	0.32802
HD171620 . . .	6	0.970	0.17920	0.94143	0.68549
G22-6	5	0.950	0.02783	0.86802	0.91052
G184-42	5	0.584	0.86209	0.46470	0.61062
HD177095 . . .	5	0.619	0.66677	0.46470	0.63213
HD177758 . . .	5	0.442	0.88743	0.97254	0.41281
G22-20	5	0.175	0.99634	0.15084	0.00396
G142-21	5	1.021	0.17997	0.33624	0.25657
BD+41-3306 . .	5	1.064	0.16527	0.99996	0.88401
HD184499 . . .	6	0.900	0.35383	0.26428	0.15900
G208-32	5	1.238	0.00399	0.23088	0.12352
G92-19	5	0.469	0.93968	0.53516	0.33578
HD188510 . . .	12	0.956	0.36204	0.40218	0.06587
HD189558 . . .	6	0.735	0.57572	0.24656	0.82823

Table 3—Continued

Star Name	N	$\left(\frac{\sigma_{\text{rms}}}{\sigma_{\text{int}}}\right)_{\text{const}}$	$\text{Pr}(\chi^2_\nu)$	$\text{Pr}(Ku)$	$\text{Pr}(F)$
BD+23-3912	6	1.904	0.00150	0.50808	0.01675
BD-15-5584.	6	0.695	0.72131	0.80697	0.98150
G186-18	5	0.289	0.96833	0.28040	0.11043
HD192718 ..	11	29.131	0.00000	4.08e-06	0.00000
G143-43	6	0.765	0.53100	0.50808	0.41691
G24-13	5	0.568	0.67617	0.94846	0.96787
HD193901 ..	5	0.238	0.98012	0.23088	0.02123
HD194598 ..	5	1.334	0.04793	0.04238	0.06854
G24-17	5	1.106	0.01483	0.11975	0.01240
HD195137 ..	6	2.876	0.00000	0.02138	0.00016
G144-9	5	0.274	0.98826	0.94846	0.26375
LP755-059 ..	5	0.620	0.76200	0.60753	0.77593
HD196892 ..	5	0.566	0.58181	0.98733	0.87411
BD+04-4551	4	0.824	0.37187	0.21669	0.34402
G25-5	5	0.594	0.76051	0.86802	0.59337
G144-52	5	0.693	0.68567	0.81241	0.78072
G187-18	5	1.891	0.00504	0.07288	0.01610
HD201889 ..	3	0.945	0.16323	...	0.82159
HD201891 ..	10	0.809	0.44775	0.97386	0.82647
G25-29	7	1.827	0.00382	0.12951	0.00091
G126-36	5	1.602	0.01637	0.28382	0.14937
LP819-002 ..	5	0.425	0.92125	0.33624	0.53348
HD210295 ..	6	4.521	0.00000	0.00115	5.79e-14
G241-7	4	0.215	0.98232	0.51650	0.08319
G241-18	5	0.913	0.21687	0.97254	0.75766
G27-44	7	6.330	0.00000	0.00026	5.25e-16
G28-15	5	0.390	0.91533	0.53516	0.23799
G28-16	3	0.886	0.22738	...	0.11421
G28-17	5	1.290	0.02682	0.81241	0.49498
G241-42	7	0.673	0.68856	0.53316	0.34534
G28-43	6	13.597	0.00000	0.00014	0.00000

Table 3—Continued

Star Name	N	$\left(\frac{\sigma_{\text{rms}}}{\sigma_{\text{int}}}\right)_{\text{const}}$	$\text{Pr}(\chi^2_\nu)$	$\text{Pr}(Ku)$	$\text{Pr}(F)$
G28-48....	5	0.827	0.49691	0.86802	0.35438
G29-20....	5	1.475	4.69e-05	0.67959	0.08443
G68-10....	5	1.392	0.04810	0.91370	0.44171
G68-30....	7	1.008	0.11101	0.97720	0.76166
G157-93...	3	2.227	0.00216	...	0.27765

Note. — χ^2 -test, F -test, and Ku -test for the complete sample.

Table 4. Test for long-term trends

Star Name	N	$\left(\frac{\sigma_{\text{rms}}}{\sigma_{\text{int}}}\right)_{\text{const}}$	Slope $\text{m s}^{-1} \text{ yr}^{-1}$	F	$P(F)$	$\left(\frac{\sigma_{\text{rms}}}{\sigma_{\text{int}}}\right)_{\text{lin}}$	$Pr(\chi^2_{\nu})_{\text{lin}}$
G30-56....	5	3.08	-35.63 ± 5.87	4.8	0.15802	1.57	0.00815
G158-102..	5	0.71	4.23 ± 8.83	1.3	0.82039	0.71	0.61624
HD3567...	3	1.25	74.43 ± 35.57	7.3	0.24196	0.57	0.41505
G270-49...	5	1.07	-19.16 ± 9.23	9.3	0.05290	0.39	0.87903
G70-17....	5	0.66	2.02 ± 10.11	1.0	0.99317	0.73	0.50310
G2-19.....	5	1.10	-24.25 ± 10.65	2.2	0.45587	0.82	0.30685
HD7424...	6	35.17	-417.02 ± 4.66	1000.	3.28e-07	1.21	0.17720
G271-34...	5	1.22	-25.12 ± 9.86	13.	0.02939	0.38	0.81465
HD10519..	3	0.65	31.88 ± 27.85	280.	0.00712	0.05	0.94815
G133-35...	3	2.91	108.20 ± 20.33	12.	0.15232	1.02	0.20236
G159-5....	6	0.86	9.24 ± 9.69	1.3	0.80679	0.84	0.50249
G272-125..	3	1.47	60.21 ± 20.07	68.	0.02916	0.22	0.79642
G74-5.....	5	1.38	-8.84 ± 4.90	1.5	0.71136	1.27	0.02885
BD-01-306	5	1.71	10.87 ± 5.29	1.0	0.97229	1.94	0.00162
G94-49....	4	1.83	6.17 ± 4.73	1.2	0.90353	2.28	0.00097
G4-10.....	5	1.49	16.96 ± 4.75	1.0	0.97150	1.69	0.00061
G94-70....	5	1.07	-0.67 ± 4.76	1.0	0.99891	1.20	0.14662
G36-28....	7	2.11	-5.21 ± 1.15	1.7	0.52877	1.74	6.31e-05
G76-30....	5	1.16	7.45 ± 4.78	1.7	0.62744	1.00	0.13957
HD19445..	6	1.10	0.52 ± 3.28	1.0	0.99484	1.21	0.11678
G77-35....	4	0.77	4.76 ± 6.93	1.1	0.95506	0.85	0.11443
G77-37....	5	1.87	0.37 ± 4.91	1.0	0.99734	2.10	0.00067
G78-41....	3	3.36	18.56 ± 3.59	19.	0.10203	0.95	0.15805
G80-15....	5	1.16	9.89 ± 6.05	1.4	0.76946	1.11	0.17939
HD23439A	5	1.14	11.52 ± 3.49	1.3	0.80477	1.46	0.34164
HD25329..	4	2.88	27.24 ± 3.91	1.5	0.75792	4.03	0.00000
G8-16.....	3	0.58	-5.29 ± 7.92	4.9	0.33834	0.32	0.52849
G82-5.....	3	2.22	18.41 ± 5.18	9.6	0.18926	0.88	0.20743
G85-17....	3	0.74	4.71 ± 4.88	630.	0.00317	0.04	0.94985
G83-50....	5	0.86	0.75 ± 1.94	1.1	0.95983	0.94	0.18127

Table 4—Continued

Star Name	N	$\left(\frac{\sigma_{\text{rms}}}{\sigma_{\text{int}}}\right)_{\text{const}}$	Slope $\text{m s}^{-1} \text{ yr}^{-1}$	F	$P(F)$	$\left(\frac{\sigma_{\text{rms}}}{\sigma_{\text{int}}}\right)_{\text{lin}}$	$Pr(\chi^2)_{\text{lin}}$
G248-45...	3	0.41	1.22 ± 5.18	1.1	0.95263	0.48	0.53791
G102-27...	3	1.05	8.40 ± 4.75	3300.	0.00059	0.022	0.97435
G100-43...	3	0.89	7.05 ± 4.81	79.	0.02496	0.12	0.85662
G192-18...	3	0.89	8.79 ± 5.95	2.1	0.63659	0.75	0.31718
G101-34...	3	1.37	-7.40 ± 3.07	20.	0.09478	0.37	0.60918
G249-49...	5	0.99	-2.99 ± 1.59	1.3	0.82722	0.99	0.47796
HD46341..	3	0.74	-4.75 ± 3.50	27.	0.07197	0.18	0.82887
G103-53...	4	2.14	11.13 ± 4.22	2.1	0.54679	1.69	0.00414
G107-43...	3	0.98	5.89 ± 4.73	6.8	0.25758	0.46	0.47304
G110-38...	4	0.44	3.64 ± 8.66	1.4	0.78489	0.43	0.71471
G193-33...	5	1.01	-6.86 ± 4.83	2.0	0.52986	0.81	0.41448
G87-27....	5	1.29	5.75 ± 3.03	1.1	0.91786	1.52	0.04012
G88-20....	7	1.43	-5.38 ± 1.84	2.7	0.24746	0.93	0.29438
G88-31....	6	1.27	-4.08 ± 2.92	1.9	0.50036	1.01	0.38429
G88-40....	4	0.71	-6.49 ± 5.77	2.3	0.52160	0.55	0.65658
HD64090..	8	0.75	-3.80 ± 2.43	1.7	0.50290	0.61	0.91313
G193-80...	5	0.88	-5.35 ± 5.08	1.0	0.99765	0.98	0.26258
G9-47.....	7	1.77	5.00 ± 3.45	1.2	0.79894	1.71	0.00125
G116-15...	5	0.90	-2.79 ± 3.81	1.1	0.96003	0.97	0.27846
G235-45...	5	0.69	0.53 ± 3.70	1.0	0.97967	0.75	0.32994
G42-34....	5	0.86	7.53 ± 3.75	1.3	0.81835	0.85	0.36435
G44-6.....	5	1.20	-1.66 ± 0.93	1.7	0.60238	1.02	0.44742
HD94028..	8	1.07	-4.15 ± 2.18	1.9	0.42227	0.83	0.59807
G122-23...	5	1.58	-3.75 ± 5.36	1.0	0.99493	1.76	0.00685
HD103095.	6	1.03	9.05 ± 7.67	1.2	0.85797	1.04	0.20137
G122-57...	6	1.12	-1.32 ± 3.63	1.0	0.98794	1.21	0.07963
G11-36....	4	1.32	-4.05 ± 9.00	1.1	0.91814	1.43	0.04182
G59-1.....	4	1.92	44.34 ± 12.90	11.	0.07645	0.65	0.54552
G197-45...	6	5.59	-46.84 ± 3.22	24.	0.00327	1.25	0.14171
G237-48...	6	1.00	-13.30 ± 7.95	2.2	0.40227	0.73	0.55592

Table 4—Continued

Star Name	N	$\left(\frac{\sigma_{\text{rms}}}{\sigma_{\text{int}}}\right)_{\text{const}}$	Slope $\text{m s}^{-1} \text{ yr}^{-1}$	F	$P(F)$	$\left(\frac{\sigma_{\text{rms}}}{\sigma_{\text{int}}}\right)_{\text{lin}}$	$Pr(\chi^2)_{\text{lin}}$
G197-51 ...	6	1.27	-7.94 ± 3.75	1.6	0.60210	1.08	0.10199
G59-18	4	1.68	-20.03 ± 8.05	2.8	0.42431	1.17	0.12393
G123-29 ...	10	0.57	0.61 ± 2.13	1.0	0.98541	0.60	0.93198
G13-38	5	0.98	-5.35 ± 10.84	1.0	0.97868	1.08	0.20164
G60-26	4	1.97	-33.59 ± 8.68	11.	0.07669	0.67	0.59244
G14-5	7	1.74	1.95 ± 0.67	2.2	0.37227	1.28	0.04621
G164-34 ...	5	0.53	-3.12 ± 4.85	1.6	0.66255	0.47	0.84662
G237-84 ...	9	4.75	23.58 ± 1.72	50.	9.76e-06	0.71	0.83459
G62-9	4	0.79	-11.75 ± 12.43	1.7	0.68390	0.70	0.48697
G61-38	4	0.94	-17.19 ± 9.29	3.6	0.31755	0.56	0.69178
G63-5	7	4.50	12.37 ± 1.07	28.	0.00074	0.91	0.63043
BD-22-3557	6	0.92	-4.97 ± 5.61	1.5	0.68900	0.83	0.49584
G63-44	7	1.89	4.76 ± 1.04	6.0	0.04572	0.83	0.49235
G63-46	4	0.29	-7.22 ± 11.12	23.	0.02819	0.069	0.99408
G135-46 ...	9	31.02	198.65 ± 2.14	250.	1.69e-08	2.07	7.74e-07
HD126681 .	6	1.29	-7.54 ± 4.22	1.1	0.89095	1.32	0.05014
G66-22	4	0.69	-5.76 ± 11.02	1.0	0.98318	0.78	0.44542
G223-82 ...	3	0.82	-2.56 ± 8.54	1.0	0.99744	1.01	0.21263
G178-50 ...	5	0.83	3.15 ± 3.37	1.4	0.75423	0.79	0.52058
G151-10 ...	7	1.32	-11.35 ± 3.73	1.2	0.86197	1.33	0.015221
G66-51	6	1.50	-6.29 ± 2.73	1.8	0.53313	1.22	0.19797
G179-11 ...	5	1.95	-0.86 ± 1.35	1.0	0.99183	2.17	0.00082
G66-55	6	0.47	-1.03 ± 5.56	1.1	0.92613	0.49	0.86423
G15-7	6	0.92	-0.41 ± 4.82	1.0	0.99004	1.00	0.32974
HD134439 .	6	1.05	9.76 ± 4.04	3.0	0.25396	0.66	0.78919
HD134440 .	6	1.01	5.82 ± 3.42	1.7	0.56879	0.84	0.39732
LHS3038 ..	6	0.72	-2.88 ± 4.61	1.3	0.79662	0.69	0.62699
G179-22 ...	5	1.36	-7.09 ± 2.74	1.3	0.81771	1.35	0.10288
G16-13	5	1.38	-14.43 ± 4.98	11.	0.04236	0.47	0.80756
G153-21 ...	5	0.77	-7.84 ± 5.49	3.1	0.29380	0.48	0.81960

Table 4—Continued

Star Name	N	$\left(\frac{\sigma_{\text{rms}}}{\sigma_{\text{int}}}\right)_{\text{const}}$	Slope $\text{m s}^{-1} \text{ yr}^{-1}$	F	$P(F)$	$\left(\frac{\sigma_{\text{rms}}}{\sigma_{\text{int}}}\right)_{\text{lin}}$	$Pr(\chi^2_{\nu})_{\text{lin}}$
G16-31	5	1.08	-28.73 ± 10.35	9.6	0.05038	0.39	0.90685
G17-10	7	0.46	-5.88 ± 5.45	1.4	0.68412	0.41	0.86620
G17-16	7	0.94	-2.83 ± 4.78	1.1	0.91742	0.97	0.35322
HD148211 . . .	3	0.40	-13.95 ± 118.19	1.0	0.97890	0.48	0.49734
HD148816 . . .	10	0.74	1.29 ± 1.27	1.4	0.65297	0.67	0.84887
G169-45	5	1.32	36.62 ± 13.38	18.	0.01547	0.34	0.92925
HD157089 . . .	13	0.91	1.98 ± 1.00	1.3	0.62189	0.81	0.81118
G19-27	18	2.46	-5.31 ± 1.11	1.6	0.37138	2.02	0.00000
G139-49	4	0.99	-7.02 ± 4.97	1.3	0.85306	1.02	0.20972
G240-68	5	0.64	-7.91 ± 6.91	1.4	0.75722	0.61	0.72024
G204-30	4	1.17	28.51 ± 12.36	78.	0.00485	0.153	0.95726
G140-33	4	0.47	0.87 ± 6.57	1.0	0.99071	0.54	0.60484
G204-49	5	1.01	-9.14 ± 5.48	1.3	0.81648	0.99	0.19597
G140-46	5	0.98	10.64 ± 8.81	1.2	0.86891	1.01	0.10264
HD171620 . . .	6	0.97	-0.76 ± 0.84	1.2	0.85488	1.16	0.15246
G22-6	5	0.95	1.90 ± 4.04	1.1	0.95898	1.09	0.01637
G184-42	5	0.58	1.95 ± 4.13	1.3	0.83271	0.58	0.78414
HD177095 . . .	5	0.62	-1.54 ± 6.54	1.0	0.98851	0.68	0.55605
HD177758 . . .	5	0.44	-0.26 ± 9.77	1.0	0.99997	0.49	0.78538
G22-20	5	0.18	0.28 ± 5.19	1.1	0.90943	0.18	0.98340
G142-21	5	1.02	-21.46 ± 11.50	1.7	0.63746	0.88	0.43448
BD+41-3306 . .	5	1.06	-10.72 ± 4.58	13.	0.03023	0.33	0.83524
HD184499 . . .	6	0.90	-2.10 ± 6.92	1.1	0.95343	0.95	0.24522
G208-32	5	1.24	-16.04 ± 5.59	2.2	0.45535	0.92	0.27136
G92-19	5	0.47	3.43 ± 7.24	2.5	0.39482	0.33	0.90945
HD188510 . . .	12	0.96	-0.05 ± 1.59	1.0	0.99512	1.00	0.29329
HD189558 . . .	6	0.73	3.52 ± 4.28	1.1	0.90674	0.76	0.55701
BD+23-3912 . .	6	1.90	-3.80 ± 3.47	1.2	0.81590	1.87	0.00333
BD-15-5584 . .	6	0.70	7.33 ± 5.24	3.0	0.25603	0.44	0.92595
G186-18	5	0.29	-4.93 ± 9.92	1.3	0.81313	0.28	0.96000

Table 4—Continued

Star Name	N	$\left(\frac{\sigma_{\text{rms}}}{\sigma_{\text{int}}}\right)_{\text{const}}$	Slope $\text{m s}^{-1} \text{ yr}^{-1}$	F	$P(F)$	$\left(\frac{\sigma_{\text{rms}}}{\sigma_{\text{int}}}\right)_{\text{lin}}$	$Pr(\chi^2_{\nu})_{\text{lin}}$
HD192718..	11	29.13	-144.65 ± 1.40	630.	2.41e-12	1.21	0.13591
G143-43....	6	0.77	3.11 ± 5.74	1.0	0.97130	0.82	0.62558
G24-13.....	5	0.57	-5.44 ± 11.67	1.0	0.99603	0.63	0.57835
HD193901..	5	0.24	-1.13 ± 3.19	1.1	0.93440	0.25	0.96901
HD194598..	5	1.33	-12.00 ± 6.29	2.0	0.52671	1.06	0.11406
G24-17.....	5	1.11	25.07 ± 7.82	8.3	0.06391	0.42	0.93369
HD195137..	6	2.88	-0.46 ± 3.69	1.0	0.99804	3.15	0.00000
G144-9.....	5	0.27	-0.92 ± 13.14	1.0	0.99964	0.30	0.95674
LP755-059..	5	0.62	2.74 ± 6.96	1.0	0.98704	0.69	0.65799
HD196892..	5	0.57	-0.37 ± 6.85	1.0	0.98465	0.62	0.49213
BD+04-4551	4	0.82	-5.45 ± 7.85	1.3	0.82607	0.82	0.26723
G25-5.....	5	0.59	6.49 ± 6.41	2.0	0.51518	0.46	0.84083
G144-52....	5	0.69	0.95 ± 6.92	1.1	0.96334	0.75	0.55338
G187-18....	5	1.89	-7.10 ± 4.26	1.4	0.75468	1.79	0.00717
HD201889..	3	0.95	14.32 ± 8.13	4.9	0.33997	0.52	0.50484
HD201891..	10	0.81	1.84 ± 1.12	1.4	0.63149	0.72	0.67613
G25-29.....	7	1.83	-7.33 ± 4.19	1.1	0.90475	1.88	0.00647
G126-36....	4	1.60	13.20 ± 7.69	1.2	0.90611	1.68	0.03098
LP819-002..	5	0.43	6.27 ± 11.82	1.6	0.66553	0.37	0.88714
HD210295..	6	4.52	-32.56 ± 3.35	3.0	0.21181	2.84	0.00000
G241-7.....	4	0.21	2.90 ± 7.54	12.	0.07007	0.07	0.99011
G241-18....	5	0.91	-1.39 ± 1.06	1.4	0.74596	0.85	0.29220
G27-44.....	7	6.33	-11.20 ± 0.78	5.7	0.03553	3.18	0.00000
G28-15.....	5	0.39	-0.92 ± 9.19	1.1	0.93926	0.41	0.85112
G28-16.....	3	0.89	65.57 ± 49.75	3.0	0.50206	0.62	0.34734
G28-17.....	5	1.29	-1.31 ± 4.38	1.0	0.98427	1.46	0.02836
G241-42....	7	0.67	-1.96 ± 2.49	1.4	0.70271	0.61	0.70227
G28-43.....	6	13.60	581.90 ± 13.94	1.7	0.59564	19.1	0.00000
G28-48.....	5	0.83	-12.26 ± 8.67	2.2	0.46471	0.62	0.72260
G29-20.....	5	1.48	-21.80 ± 5.05	2.3	0.43737	1.09	0.30461

Table 4—Continued

Star Name	N	$\left(\frac{\sigma_{\text{rms}}}{\sigma_{\text{int}}}\right)_{\text{const}}$	Slope $\text{m s}^{-1} \text{ yr}^{-1}$	F	$P(F)$	$\left(\frac{\sigma_{\text{rms}}}{\sigma_{\text{int}}}\right)_{\text{lin}}$	$Pr(\chi^2_{\nu})_{\text{lin}}$
G68-10	5	1.39	-12.72 ± 5.50	1.7	0.63723	1.21	0.27852
G68-30	7	1.01	0.23 ± 0.75	1.1	0.93749	1.05	0.06873
G157-93 . . .	3	2.23	62.42 ± 18.83	22.	0.08587	0.57	0.39496

Note. — inear RV trend tests for our sample. For each star with more than three observations, we report the values of $(\sqrt{\chi^2_{\nu}})_{\text{const}}$ (for comparison from Table 3), the slope and its formal error of a linear fit to the RV data, the F -test results, and the recomputed $(\sqrt{\chi^2_{\nu}})_{\text{lin}}$ and $Pr(\chi^2_{\nu})_{\text{lin}}$ on the post-fit residuals.

Table 5. Radial velocity measurements for stars with $\sigma_{\text{rms}}/\bar{\sigma}_{\text{int}} \lesssim 3.0$.

BJD – 2,400,000	Radial Velocity (m s ⁻¹)	σ_{RV} (m s ⁻¹)
G 30-56		
53192.05224	0.4	5.5
53209.09366	28.3	7.0
53210.07438	18.7	8.8
53569.08494	–24.4	5.3
53570.07546	–23.1	7.9
G 158-102		
53192.07375	–14.3	12.2
53209.07767	1.6	12.1
53210.05681	4.0	6.0
53569.10203	5.1	9.6
53570.09542	3.6	10.8

Note. — We intend for this table to appear in its entirety in the electronic version of the journal. A portion is shown here to illustrate its format. The data are also available from the authors upon request.

Table 6. Radial velocity measurements for stars with linear trends.

BJD - 2,400,000	Radial Velocity (m s ⁻¹)	σ_{RV} (m s ⁻¹)
HD 7424		
53192.10039	241.1	6.4
53209.12624	225.2	3.7
53210.11312	224.9	7.6
53569.11138	-180.7	8.5
53570.10677	-178.1	6.0
53684.76920	-332.4	7.8
G 237-84		
51291.99768	-77.6	10.6
51293.96887	-89.0	14.6
51547.17281	-53.4	11.0
52679.05301	26.1	12.6
52680.04800	22.4	11.9
52811.76697	16.7	10.7
53161.78931	38.6	10.4
53191.73366	42.6	8.9
53568.74194	73.5	12.8
G 197-45		
52679.03966	51.3	8.6
52680.02637	48.6	4.9
52811.75498	9.4	8.2
53161.76507	-17.5	7.3
53207.73066	-27.5	7.6
53568.74707	-64.4	7.5
G 63-5		
50864.03514	-52.9	14.2
50866.00624	-48.0	11.8
51007.80053	-28.4	9.0
51548.09345	-9.6	7.7
53161.89205	38.9	6.7

Table 6—Continued

BJD - 2,400,000	Radial Velocity (m s ⁻¹)	σ_{RV} (m s ⁻¹)
53191.82188	37.6	4.2
53568.77818	62.5	12.8
G 135-46		
52678.12921	-213.3	6.6
52679.09727	-210.3	7.8
52680.08853	-212.4	6.3
52811.80232	-141.6	4.1
53161.81140	72.4	6.0
53191.82815	92.1	4.9
53206.74503	86.6	6.3
53568.79557	262.9	6.3
53569.77774	263.6	5.5
G 204-30		
52812.02781	-18.2	10.0
52920.70008	-5.7	9.7
53161.99866	10.1	11.1
53206.89863	13.8	13.2
HD 192718		
51398.90265	588.0	8.0
51400.91461	584.5	11.9
52811.92588	35.1	11.0
52854.93152	22.4	8.6
52920.82402	-12.8	9.8
53162.04705	-101.7	8.5
53191.93307	-109.6	13.4
53208.94383	-111.4	9.5
53568.96500	-288.7	13.2
53569.97918	-295.2	10.3
53684.69217	-310.6	8.6

Table 7. Radial velocity measurements for stars with non-linear trends.

BJD - 2,400,000	Radial Velocity (m s ⁻¹)	σ_{RV} (m s ⁻¹)
HD 210295		
53209.04688	9.4	5.5
53210.03125	64.6	10.7
53569.00391	37.0	8.7
53569.98828	18.8	15.8
53949.98438	-50.0	7.1
53951.05469	-59.6	8.8
53952.08203	-20.2	8.4
G 27-44		
50668.01562	31.5	7.3
50670.01562	32.2	8.9
51008.06641	41.4	3.7
51038.98438	22.9	7.5
51545.72266	26.6	14.5
53162.06250	0.0	6.4
53569.00781	-80.1	8.4
53952.08984	-74.7	10.7
G 28-43		
53162.08430	-401.4	7.3
53209.05709	51.8	43.9
53210.03967	164.1	38.5
53569.03491	402.8	18.5
53570.02176	449.4	25.5
53684.75181	-666.8	46.1

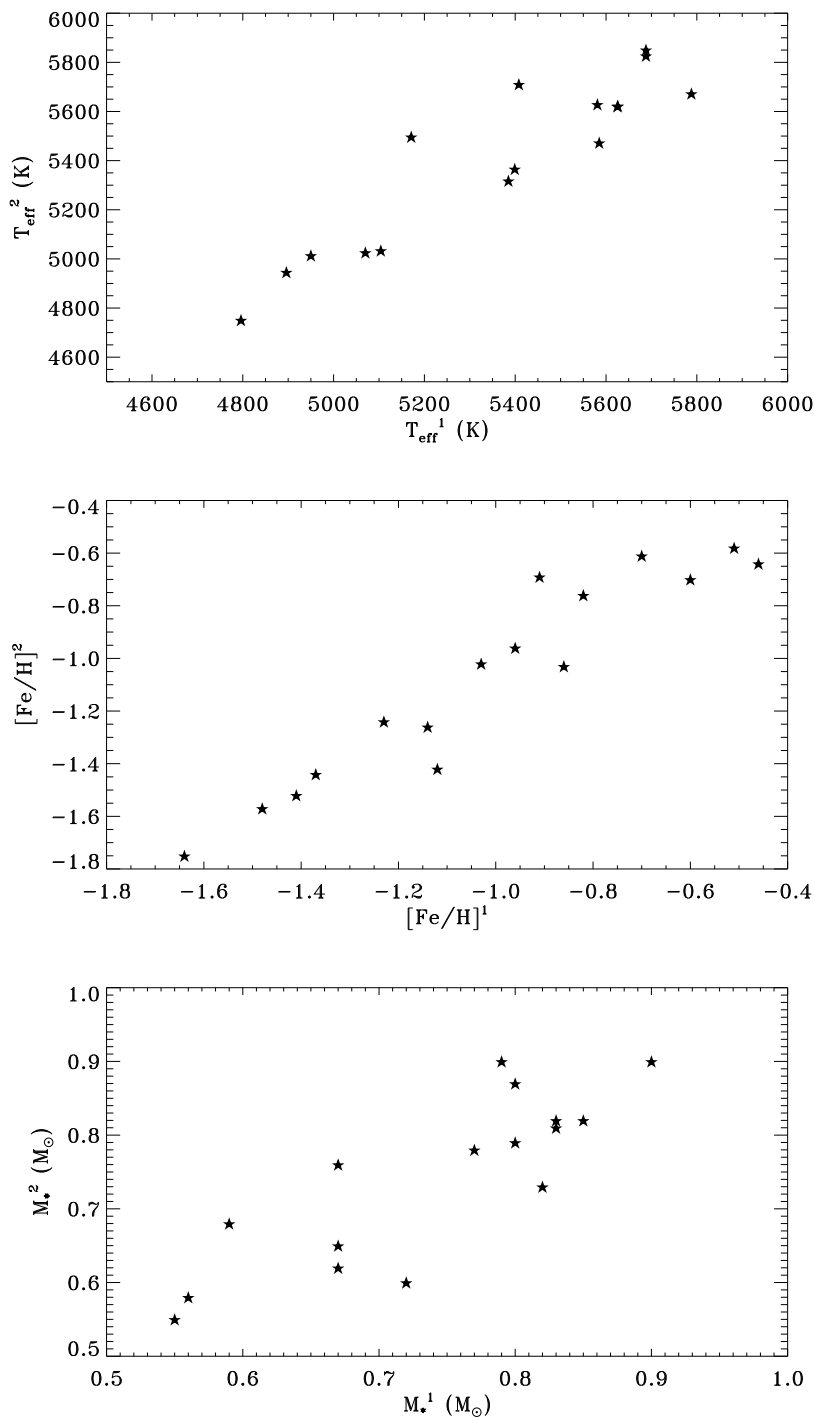


Fig. 1.— Comparison between the values of T_{eff} , $[\text{Fe}/\text{H}]$, and M_* (top, center, and lower panel, respectively) for the objects in common between our program stars (with superscript 2 on the y -axis) and the SPOCS database (with superscript 1 on the x -axis) described in Valenti & Fischer (2005) and Takeda et al. (2007).

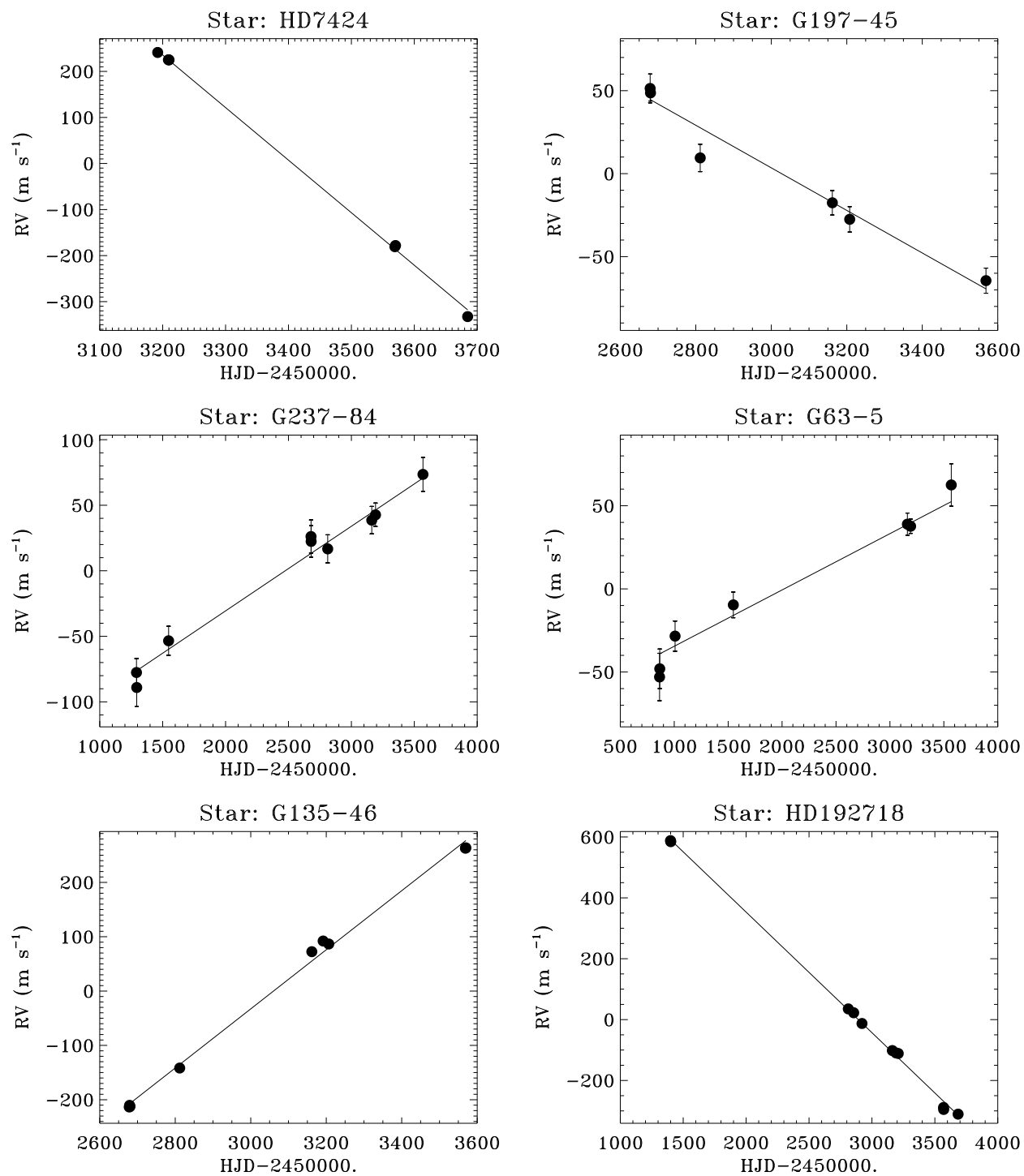


Fig. 2.— Linear fits (solid lines) to the RV data of six RV variables: HD 7424, G 197-45, G 237-84, G 63-5, G 135-46, and HD 192718.

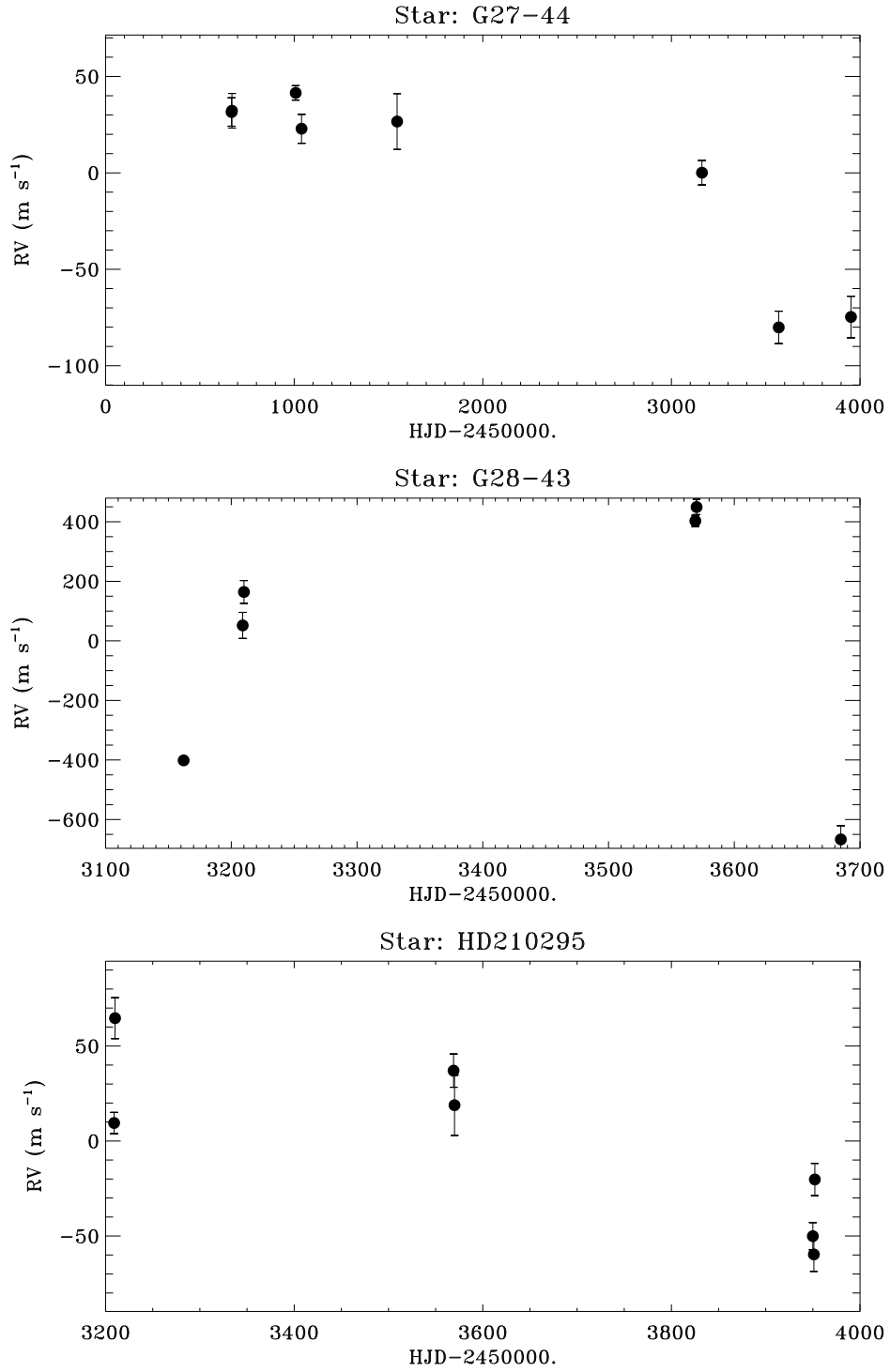


Fig. 3.— Radial velocity as a function of time for three stars exhibiting significant non-linear RV variability: G 27-44 (upper panel), G 28-43 (middle panel), and HD 210295 (lower panel).

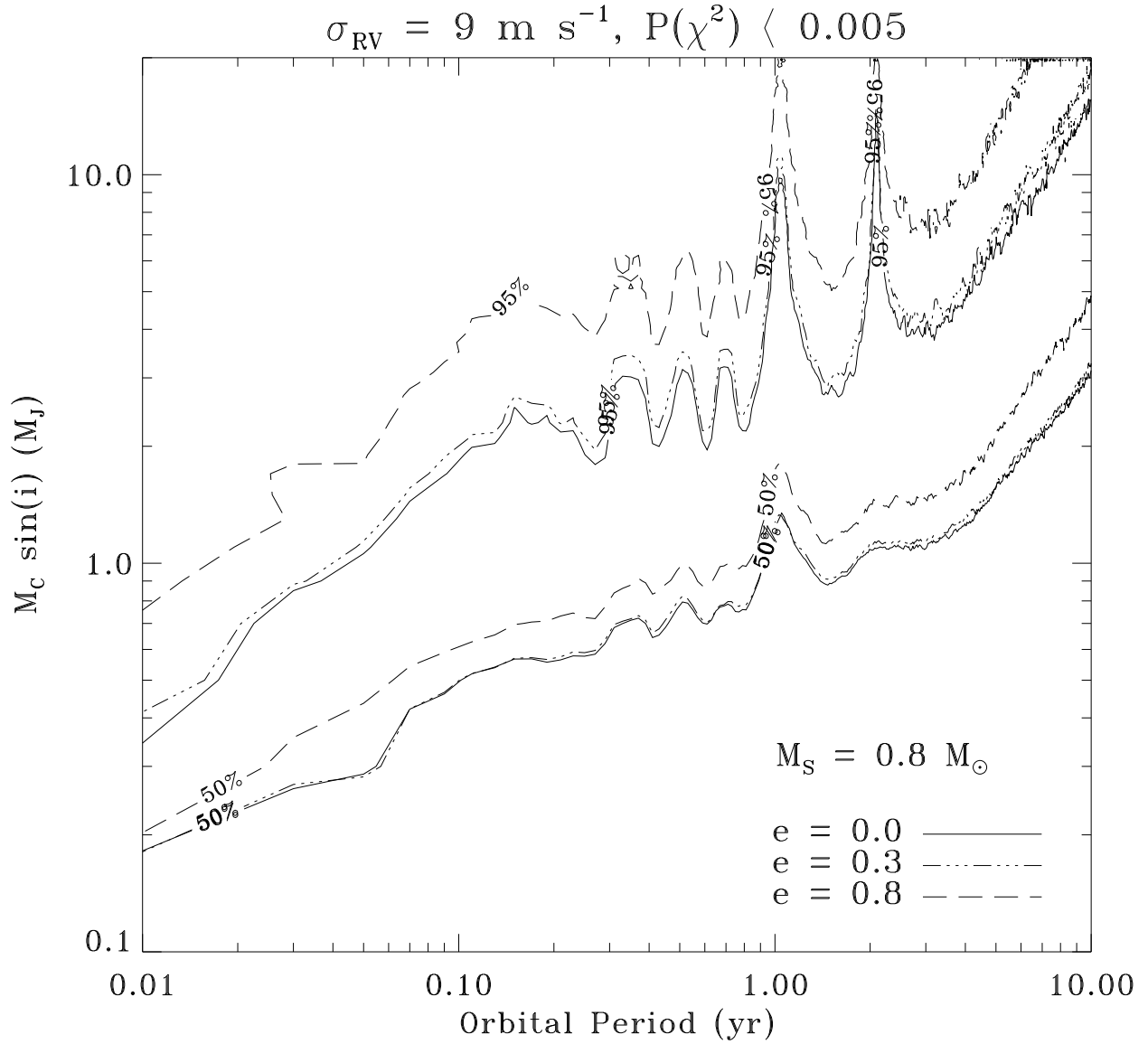


Fig. 4.— Survey completeness for companions of given mass, orbital period, and eccentricity. The limits shown are for 50% and 95% completeness and for three realizations with different values of eccentricity.

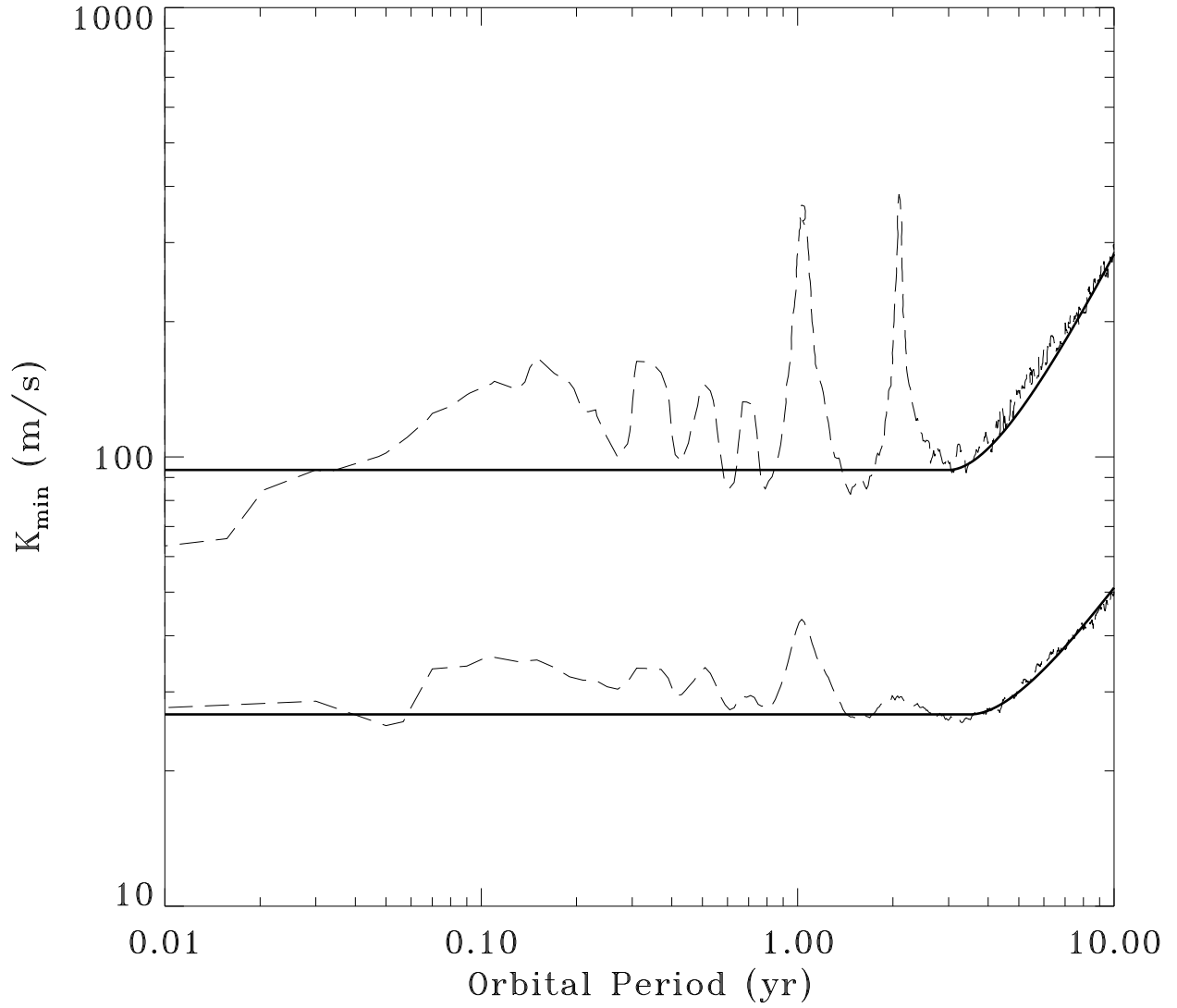


Fig. 5.— Radial velocity detectability threshold for 50% and 95% detection efficiency (lower and upper dashed lines, respectively). The solid lines represent analytical results using the Cumming (2004) formalism.

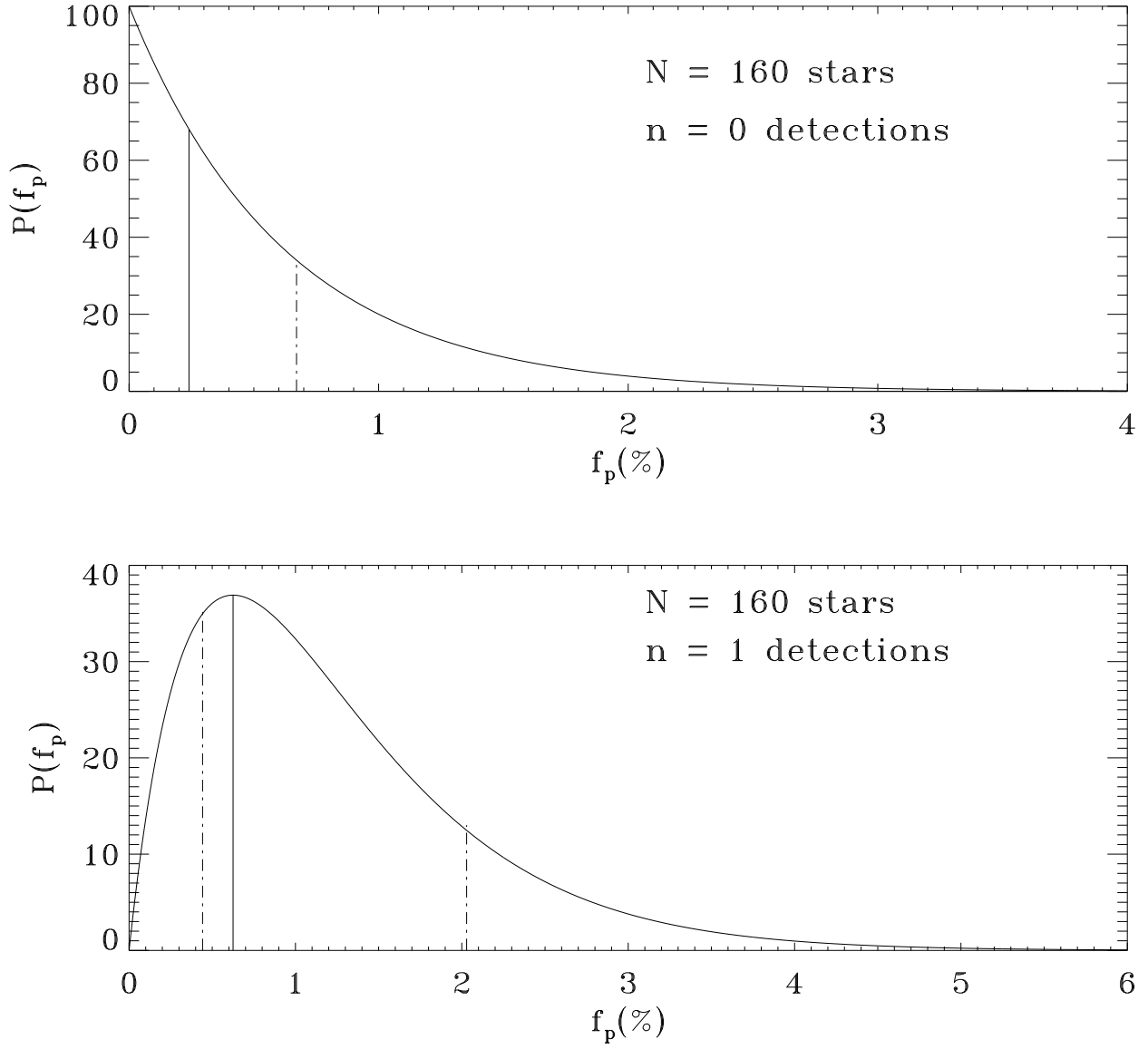


Fig. 6.— Probability function for a given sample size and true companion frequency, and the case of no detections (upper panel) and one successful detection (lower panel).

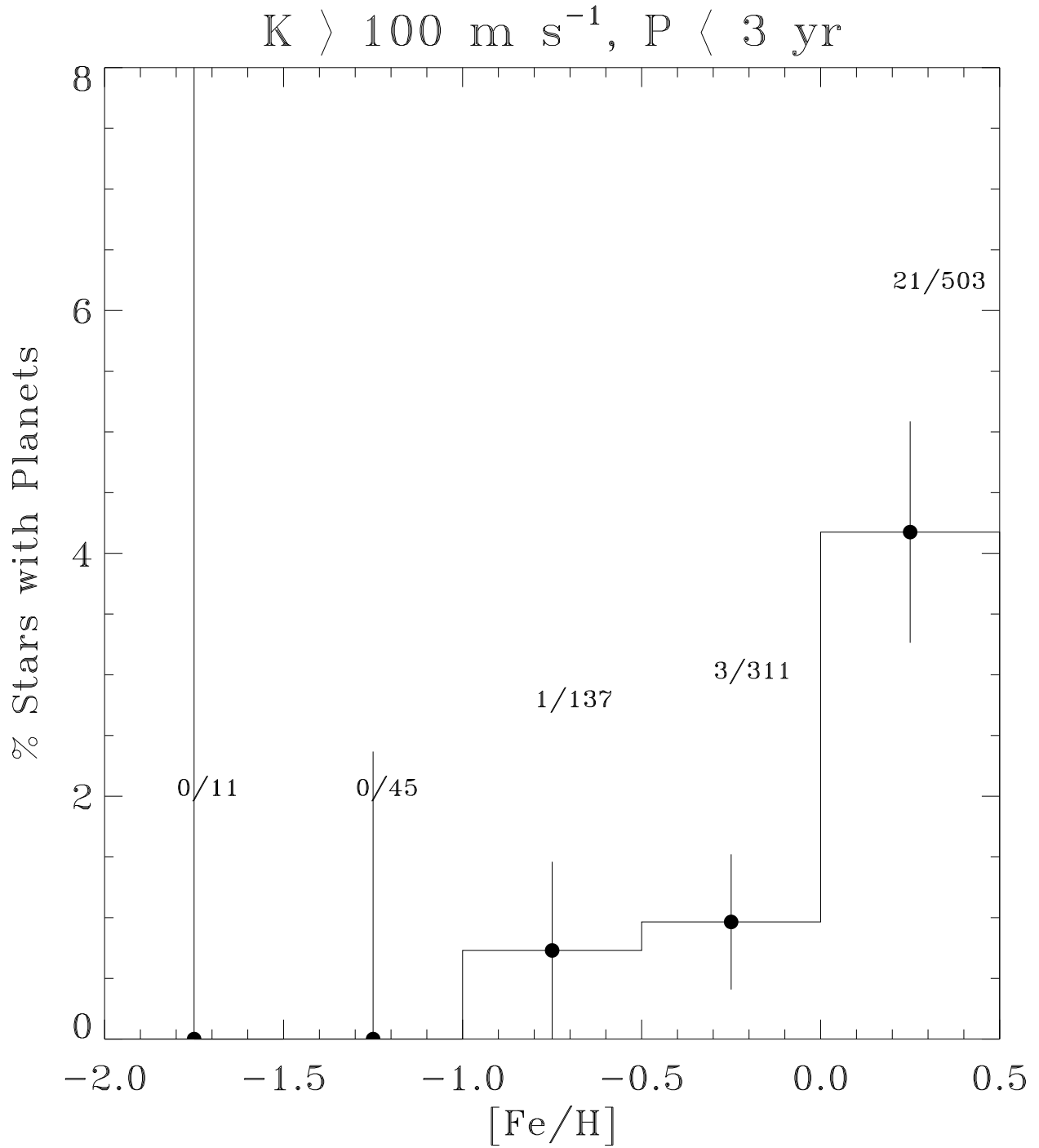


Fig. 7.— Percentage of giant-planet hosting stars as a function of metallicity (0.5 dex bins) for the sample constructed combining our survey stars with those from the Fischer & Valenti (2005) database that have $K > 100 \text{ m s}^{-1}$ and $P < 3 \text{ yr}$.

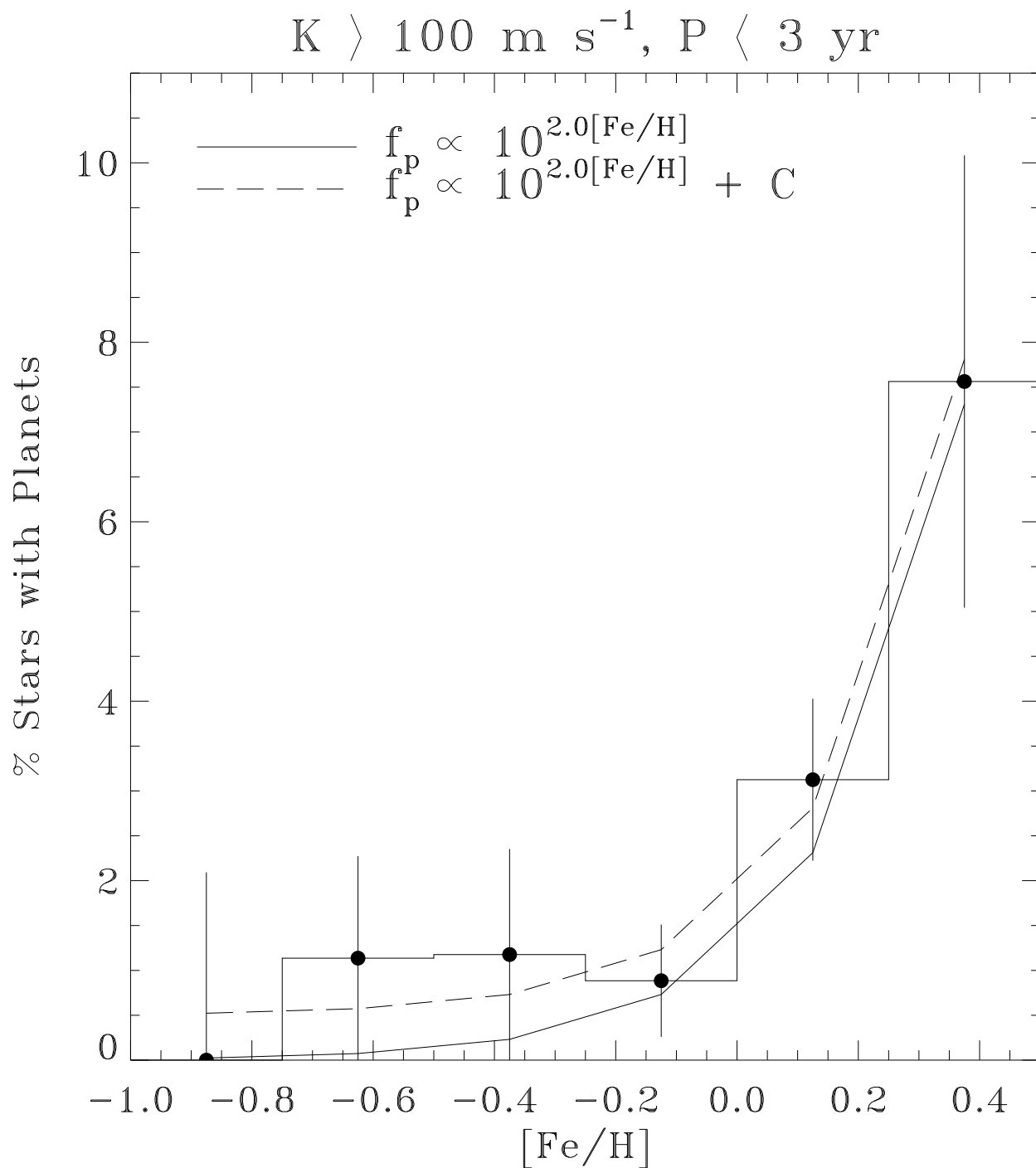


Fig. 8.— Same as Figure 7, but divided into 0.25 dex metallicity bins. The increasing trend in the fraction of stars with planets as a function of metallicity is well fitted with a power law, but the data are compatible with a constant occurrence rate $f_p \simeq 1\%$ for $[\text{Fe}/\text{H}] \lesssim 0.0$.